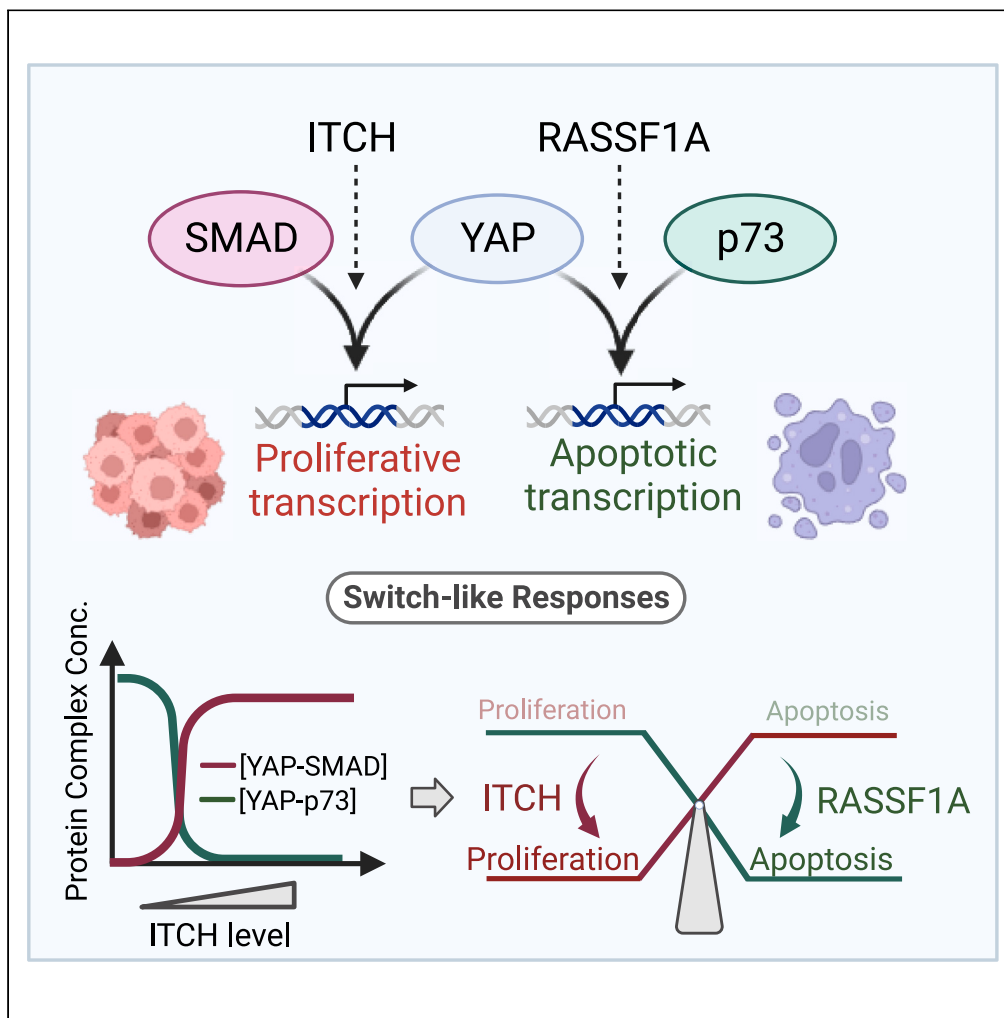**Article**

Integrative modeling and analysis of signaling crosstalk reveal molecular switches coordinating Yes-associated protein transcriptional activities

Milad Ghomlaghi, Mandy Theocharous, Nhan Hoang, ..., Eric O' Neill, Tao Zhang, Lan K. Nguyen

lan.k.nguyen@monash.edu

Highlights

A new mathematical model of TGF-β/Hippo signaling crosstalk, focusing on YAP complexes

Integrative modeling reveals switch-like behavior of the YAP-SMAD and YAP-p73 complexes

RASSF1A and ITCH are key switch regulators; increasing ITCH sustains YAP-SMAD activity

Protein levels affect switch features, highlighting cellular context in YAP regulation

Article

Integrative modeling and analysis of signaling crosstalk reveal molecular switches coordinating Yes-associated protein transcriptional activities

Milad Ghomlaghi,[1,2] Mandy Theocharous,[1,2] Nhan Hoang,[1,2] Sung-Young Shin,[1,2] Alex von Kriegsheim,[3] Eric O' Neill,[4] Tao Zhang,[1,2] and Lan K. Nguyen[1,2,5,*]

SUMMARY

The transcriptional co-activator YAP forms complexes with distinct transcription factors, controlling cell fate decisions, such as proliferation and apoptosis. However, the mechanisms underlying its context-dependent function are poorly defined. This study explores the interplay between the TGF-β and Hippo pathways and their influence on YAP's association with specific transcription factors. By integrating iterative mathematical modeling with experimental validation, we uncover molecular switches, predominantly controlled by RASSF1A and ITCH, which dictate the formation of YAP-SMAD (proliferative) and YAP-p73 (apoptotic) complexes. Our results show that RASSF1A enhances the formation of apoptotic complexes, whereas ITCH promotes the formation of proliferative complexes. Notably, higher levels of ITCH transform YAP-SMAD activity from a transient to a sustained state, impacting cellular behaviors. Extending these findings to various breast cancer cell lines highlights the role of cellular context in YAP regulation. Our study provides new insights into the mechanisms of YAP transcriptional activities and their therapeutic implications.

INTRODUCTION

The Hippo signaling pathway plays a critical role in the regulation of tissue homeostasis, organ size, cell proliferation, and apoptosis.[1–5] Dysregulation of the pathway in humans has been linked to cellular hyperproliferation, invasion and metastasis that are hallmarks of oncogenesis.[6] Yes-associated protein (YAP) is a primary transcriptional effector of the Hippo pathway, located downstream of the core pathway kinases MST1/2 and LATS1/2.[7] Although possessing transcriptional activity, YAP cannot bind DNA. Instead, it interacts with a number of DNA-binding transcription factors (TFs), including TEAD, SMAD, RUNX, and p73, to form transcriptionally active complexes to induce the target genes' expression. While it is clear that YAP is an important positive regulator of pro-proliferative and anti-apoptotic genes, growing evidence suggests that in mammals, YAP has a dual role and can either inhibit or promote apoptosis.[8] This seems to underpin the ability of YAP to function both as an oncogene and a tumor suppressor, depending on the biological context.[8] However, the molecular mechanisms by which YAP coordinates its context-dependent function remain incompletely understood. Clearly, improved mechanistic understanding of this process may help identify novel strategies targeting Hippo-YAP pathway dysregulation in human cancer.

The dichotomous function of YAP stems in part from its capacity to bind and form complexes with different TFs that have distinct biological functions. For example, members of the TEAD transcriptional factor family are major binding partners of YAP, which upon YAP binding, activates target genes involved in cell proliferation.[9] YAP also binds SMAD and YAP/SMAD transcriptional complexes to contribute to oncogenic phenotypes.[10,11] On the other hand, YAP can bind to DNA-binding tumor suppressors including RUNXs and p73 to mediate its anti-oncogenic function. RUNX3 interacts directly with TEAD, which markedly reduces TEAD's DNA-binding ability and disrupts YAP-TEAD mediated oncogenic gene expression in gastric cancer.[12] RUNX1 and 3 are also negative regulators of the oncogenic function of YAP in breast cancer.[13] To restrict cell growth or respond to stress, the Hippo pathway increases YAP affinity for p73 to promote the transcription of pro-apoptotic genes.[14] In this context, we and others have identified the tumor suppressor and scaffold protein RASSF1A as a key positive mediator of YAP-p73 complex formation via signaling through the MST1/2-LATS1/2 kinase cassette.[15–18] Despite the increasing evidence supporting that YAP may coordinate its oncogenic or tumor-suppressing function by switching between different binding partners, how this occurs remains poorly defined.

[1]Department of Biochemistry and Molecular Biology, School of Biomedical Sciences, Monash University, Clayton, VIC 3800, Australia
[2]Biomedicine Discovery Institute, Monash University, Clayton, VIC 3800, Australia
[3]Edinburgh Cancer Research UK Centre, Institute of Genetics and Molecular Medicine, The University of Edinburgh, Crewe Road South, Edinburgh EH4 2XR, UK
[4]CRUK/MRC Institute for Radiation Oncology and Department of Oncology, University of Oxford, Oxford OX3 7DQ, UK
[5]Lead contact
*Correspondence: lan.k.nguyen@monash.edu

The coordination of distinct YAP-TF complexes and ensuing cell fates is achieved through signaling pathway crosstalk. We previously showed that crosstalk between the RASSF1A/MST2/LATS and RAF-1/ERK signaling modules orchestrates the decision between cell survival and apoptosis, which is mediated by signaling switches arising from intricate competing protein interactions.[2] In addition, the Hippo pathway is engaged in crosstalk with various other pathways, including RAF-1/ERK,[2,19] WNT, and PI3K/AKT.[20,21] The TGF-β/SMAD signaling pathway, which plays a critical role in various stages of tumorigenesis, also intimately interplays with Hippo-YAP signaling.[22–27] Stimulation by TGF-β triggers the dimerization and activation of the TGF-β Receptors (TGF-βR1/2), which induces the phosphorylation of SMAD2/3, complex formation with SMAD4, and translocation to the nucleus to engage DNA-binding partners and transcriptional co-activators for the transcription of target genes.[28] The nuclear-cytoplasmic shuttling of SMADs is tightly regulated and is mediated through association with YAP.[25] In the absence of YAP/TAZ, SMADs fail to accumulate in the nucleus, and TGF-β mediated transcription is disabled.[25] The YAP-SMAD complex also can bind TEAD in the nucleus and promotes TGF-β mediated tumorigenic activity.[10,11] Furthermore, we previously demonstrated that TGF-β/Hippo signaling crosstalk is further mediated by the interaction between TGF-βR1/2 and RASSF1A.[27] Upon TGF-β mediated activation of the receptors, RASSF1A is recruited to the plasma membrane (PM) together with the E3 ligase ITCH where it is ubiquitinated and degraded by ITCH. The degradation of RASS1A leads to the enhanced formation of the YAP-SMAD complex that promotes a pro-proliferative gene expression program (Figure 1A). As RASSF1A is a known regulator of YAP-p73 binding, these data suggest that RASSF1A and ITCH may coordinate the assembly of YAP complexes with the different TFs, SMAD, and p73. Yet, given the complexity of the TGF-β/Hippo crosstalk network, a systematic understanding of the dynamic regulation of the YAP-SMAD/p73 complexes is lacking.

In this study, we leveraged an integrative, systems-based approach, synergizing computational network modeling and experimental investigations to explore the dynamic formation and transition of YAP transcriptional complexes. A novel mechanistic model was constructed to understand the interaction between the TGF-β and Hippo signaling pathways, with this model trained using time-resolved experimental data. Our comprehensive studies uncovered RASSF1A and ITCH as crucial regulators of the YAP-p73 and YAP-SMAD complexes. An interesting observation was that a gradual increase in ITCH expression could induce a switch-like response in the YAP-TFs complexes, where YAP abruptly transitions from binding to p73 to associating with SMAD, a shift that enhances proliferative gene expression.

The model simulations indicated that the sharpness of the switches hinges on the protein expression profiles within specific cell types. Moreover, a rise in ITCH levels can alter the temporal dynamics of the YAP-SMAD complex from a transient to a sustained response following TGF-β stimulation. Incorporating data from DepMap,[29] we further found that the critical role of ITCH in maintaining cell viability is linked to its impact on the regulation of YAP complexes. These results, together with the observation that ITCH is upregulated in various tumors[30,31] underscore its potential as a promising therapeutic target for anti-cancer treatment. Overall, our research sheds new light on the dynamic regulation of YAP-TF complexes, highlighting the functional opposition between these transcriptional units.

RESULTS

Dynamic TGF-β/Hippo signaling pathway crosstalk

To construct a dynamic mathematical model of the TGF-β/Hippo signaling crosstalk, it is crucial to understand the time-resolved interactions among the components of these pathways. To characterize their dynamic interplay, we subjected mammary epithelial MCF-10A cells to TGF-β stimulation and determined the temporal response profiles of the pathway components using immunoblot analysis. Upon TGF-β treatment, we observed a rapid and potent increase in the phosphorylation of SMAD2 and 3, an expected response that peaked around 1 h and gradually diminished at later time points (Figures 1B and S1A). This transient pattern of pSMAD2/3 aligns with previous studies, and it is likely attributed to the known negative feedback mechanism mediated by SMAD7.[32,33] Interestingly, we observed an elevated level of basal SMAD7 even before treatment, which heightened over time in response to TGF-β, triggering the negative feedback loop (Figure 1B).

In contrast, TGF-β treatment led to a significant time-dependent decrease of RASSF1A expression, as previously reported (Figures 1C and S1B), reaffirming the inhibitory impact of TGF-β stimulation on RASSF1A.[27] This decrease in RASSF1A, along with its regulatory effect on YAP-p73 transcriptional activity, is further evidenced by the reduced concentration of PUMA, an apoptotic protein whose expression is controlled by YAP-p73 (Figures 1C and S1E). Interestingly, TGF-β treatment induced a significant increase in phosphorylated YAP levels at tyrosine 357 (pY357). The level of YAP pY357 doubled at 2 h post-stimulation and became steady at 8 h post-stimulation (Figures 1C and S1C). This trend was further corroborated by an extended time-course over 24 h of TGF-β treatment (Figure 1D). YAP pY357 has been demonstrated to stabilize YAP and increase YAP affinity for p73.[34] This phosphorylation is mediated by the non-receptor tyrosine kinase c-Abl,[34–36] which is known to be regulated by TGF-β signaling.[37] Contrary to YAP pY357, we did not observe significant changes in total YAP or phosphorylated YAP at serine 127 (pS127) following TGF-β treatment (Figure S1D). Additionally, TGF-β did not impact the expression of p73 (Figures 1D and S1F).

Collectively, these findings illuminate the dynamics of TGF-β/Hippo-YAP signaling crosstalk following TGF-β stimulation, providing valuable time-resolved data for model construction. Importantly, our data indicate that TGF-β not only initiates SMAD signaling but also enhances YAP-p73 association through increased YAP pY357 (Figures 1C and S1C). This enhancement represents a novel crosstalk point between the TGF-β and Hippo-YAP pathways.

A mechanistic model of TGF-β/Hippo-Yes-associated protein signaling crosstalk

While there is clear evidence supporting the crosstalk between TGF-β and Hippo-YAP, the process by which YAP integrates these upstream signals and the intricate regulatory mechanisms to induce robust transcriptional decisions is not well understood. To address this, we sought to construct a new mathematical model of the signaling network that aims to encapsulate the complex crosstalk and regulatory mechanisms within a single, quantitative framework.
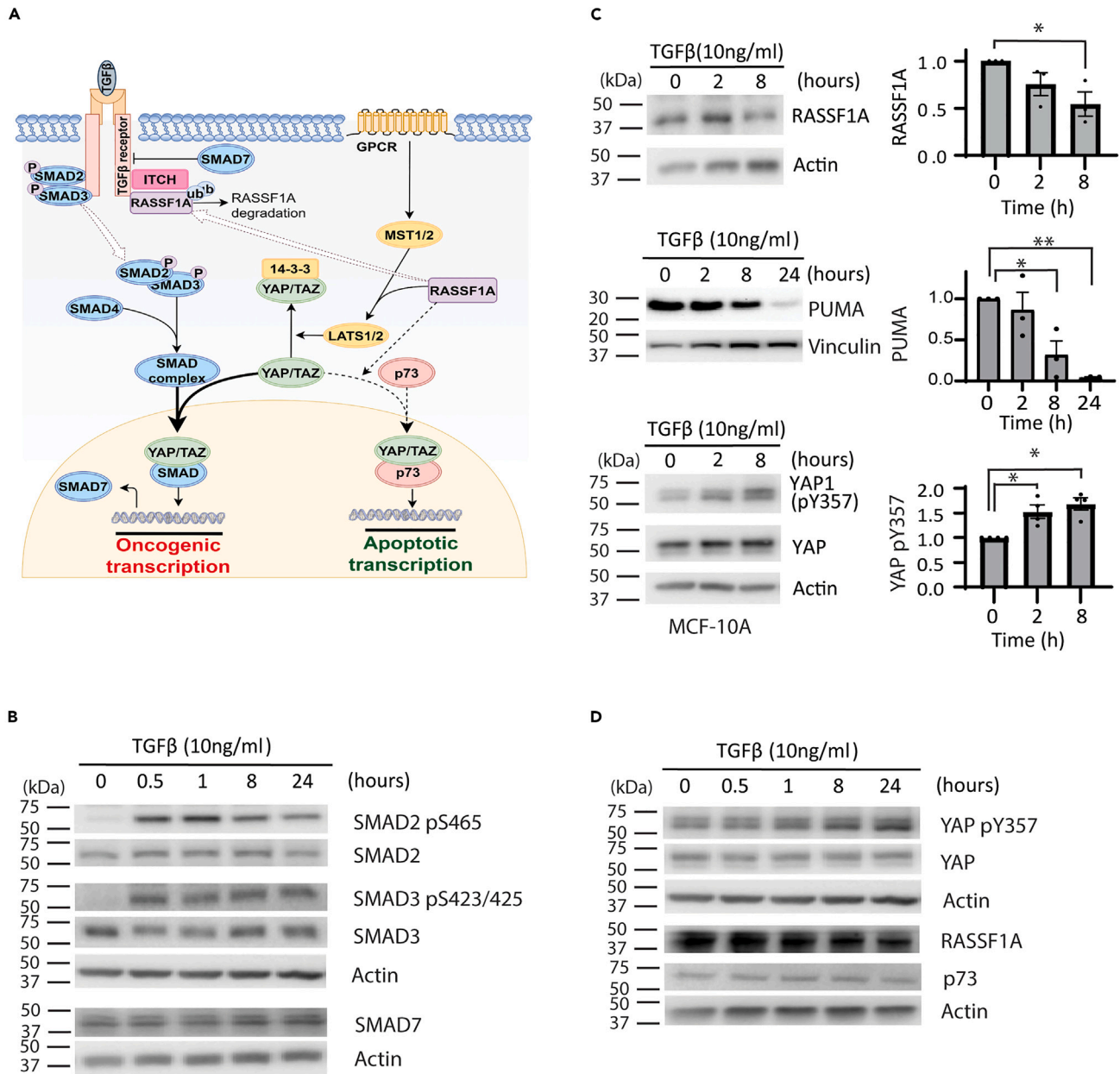
Figure 1. Characterization of the dynamic TGF-β-Hippo pathway signaling crosstalk

(A) A schematic diagram displaying the crosstalk between the TGF-β/SMAD and Hippo/RASSF1A/YAP signaling pathways.

(B) Time course analysis of TGF-β stimulation on the TGF-β/SMAD signaling pathways in the MCF-10A cells. Expression and activation of signaling proteins in 0 (untreated condition), 0.5, 1, 8 and 24 h post-treatment with 10 ng/mL of TGF-β. Lysates were immunoblotted with antibodies as specified, with actin as a loading control (n = 1, p; phosphorylated).

(C) Time course analysis of TGF-β stimulation on RASSF1A and phosphorylated and total YAP in MCF-10A cells. Expression and activation of signaling proteins in 0 (untreated condition), 2, and 8 h post-treatment with 10 ng/mL of TGF-β. Quantification of the western blot data is given on the right panels (n = 3 biological replicates). Error bars show mean $\pm$ standard deviation (SD). Continuous data differences analysis was evaluated by Student's t-test between two groups. $p < 0.05$ was considered significant. ns $p \geq 0.05$, *$p < 0.05$, **$p < 0.01$, ***$p < 0.001$, ****$p < 0.0001$.

(D) Time course analysis of TGF-β stimulation (10 ng/mL) on components of the Hippo/RASSF1A signaling axis in MCF-10A cells, as described in (C) but included 24 h stimulation (n = 1 biological replicates).

Model inputs, outputs, and reactions

A reaction schematic of the new model is presented in Figure 2A, illustrating the reactions incorporated into the model. These model reactions are further elaborated in Table S1. The main input of the model is the TGF-β ligand. In short, TGF-β stimulation causes the ligand to bind
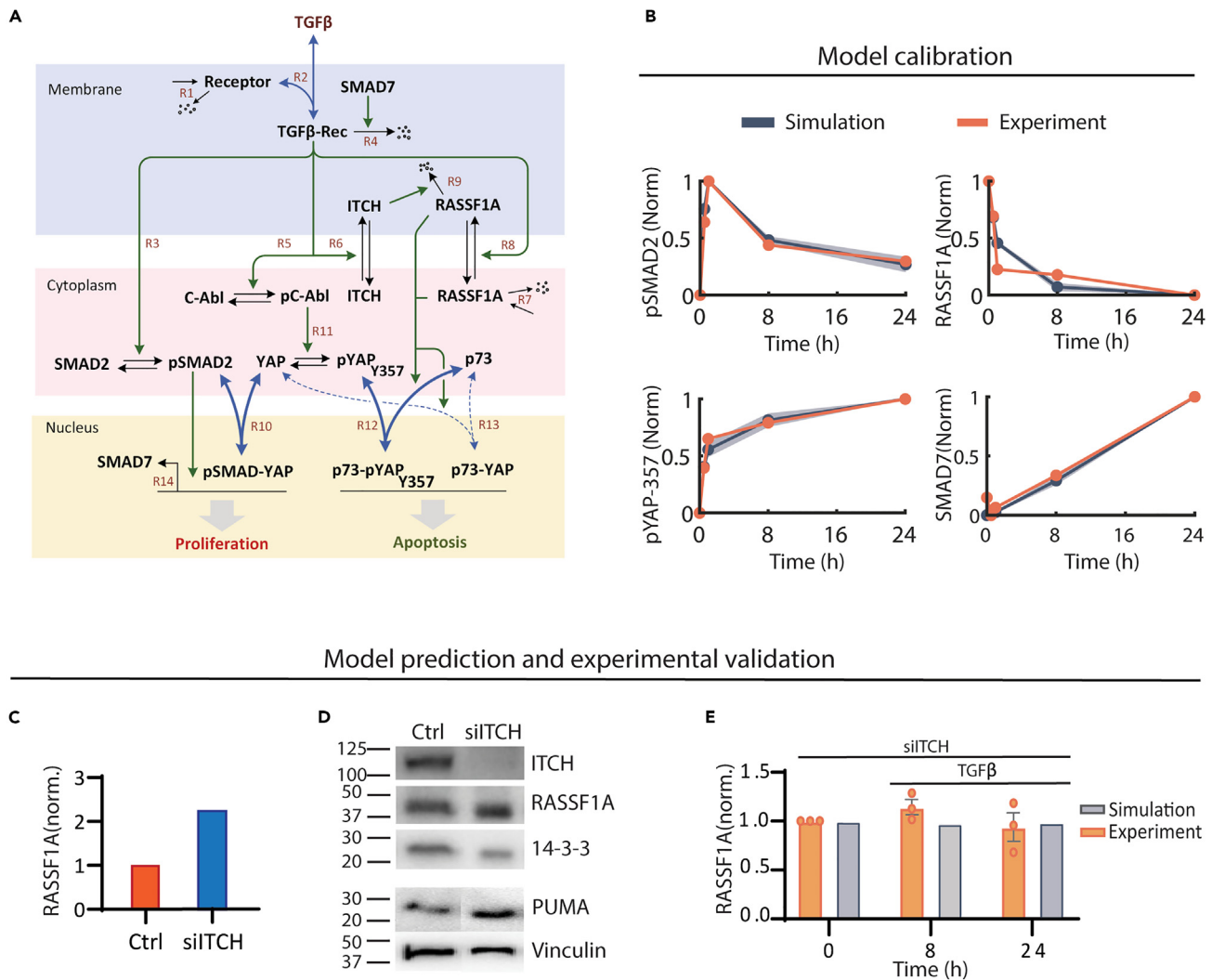
Figure 2. Construction, calibration, and validation of a new mathematical model of the TGF-β-Hippo signaling crosstalk network

(A) A reaction schematic diagram displaying the biochemical reactions included in the mathematical model of the pathway crosstalk. Detailed description of the model is given in the main text.

(B) Time-course model simulations using the best-fitted parameter sets (blue curves) in comparison with the quantified experimental data (brown curves) from Figure 1, showing strong concordance between simulation and data. A total of 11 best-fitted parameter sets obtained from model calibration were used for the simulations (solid blue line demonstrates the mean simulated curve, and shaded area shows standard deviation).

(C–E) Independent validation of the model. (C) Model simulation results predicting the upregulation of RASSF1A expression after siRNA-mediated knockdown of ITCH (right), as compared to experimental data determined using western blot (D). As a readout for YAP-p73 transcriptional activity, PUMA upregulation indicates an increase in YAP-p73 formation that is regulated by RASSF1A. RASSF1A and PUMA are measured 2 h after ITCH knockdown. Sim = simulation, Exp = experiment (n = 1 biological replicate) (E) Effect of TGF-β stimulation on RASSF1A level under ITCH knockdown condition. Simulations predict ITCH knockdown prevents RASSF1A degradation after TGF-β stimulation, which is confirmed by experimental data. Here, MCF-10A cells where ITCH has been knocked down were stimulated with TGF-β (10 ng/ml) and RASSF1A protein expression was measured by western blot (n = 3 biological replicates). Error bars show mean ± standard deviation (SD).

to and activate the TGF-β receptor (as shown in reaction R2, Figure 2A and Table S1). The receptor undergoes protein turnover through synthesis and degradation (R1). The active TGF-β receptor phosphorylates the transcriptional factors SMAD2/3, prompting their complex formation. Our data suggest that SMAD2 and 3 exhibit similar response dynamics following TGF-β treatment (Figures 1B and S2B). Therefore, for the sake of simplicity, we regard SMAD2 as the representative protein of the SMAD complex (R3).[38,39] Phosphorylated SMAD2 subsequently forms complexes with YAP and translocates to the nucleus to initiate the transcription of YAP-SMAD target genes (R10).[25]

Inside the nucleus, the YAP-SMAD complex can also associate with TEAD to form ternary complexes. However, in response to TGF-β stimulation, it is likely that SMAD, rather than TEAD, plays a leading role in driving YAP-mediated proliferative gene expression, allowing us to omit TEAD from our model for simplicity. In addition, while TGF-β-mediated transcription heavily relies on YAP,[40] phosphorylated SMAD2

is likely transcriptionally on its own. Therefore, we assume unbound pSMAD2 can also initiate transcription, albeit at a relatively slower rate compared to the YAP-SMAD complex.[40] SMAD7, a target gene of SMAD2/3 (R14), counteracts the TGF-β receptor through receptor ubiquitination and degradation, thus generating a negative feedback loop (R4).[41]

On the Hippo signaling side, RASSF1A promotes YAP-p73 binding through the activation of the kinases MST2/LATS1 (R13 and R14).[2,15] The potent TGFβ-induced YAP pY357 (Figure 1C) suggests this phosphorylation is highly dynamic and tightly regulated, necessitating explicit inclusion of YAP-pY357 in the model (R12). YAP phosphorylation at pY357 is catalyzed by the kinase c-Abl and can be dephosphorylated by inherent phosphatases to revert to its unphosphorylated state (R11). As YAP-pY357 exhibits a stronger affinity for p73 than unphosphorylated YAP,[35] we assumed a relatively smaller dissociation constant for reaction R12 compared to R13, both of which are stimulated by RASSF1A. We have previously shown that following TGF-β stimulation, the TGF-β receptor recruits both RASSF1A and the E3 ligase ITCH to the PM where ITCH degrades RASSF1A (Figure 1C).[27] The model reflects this crosstalk mechanism by incorporating the translocation of RASSF1A and ITCH from the cytoplasm to the PM (R8 and R6, Figure 2A) and the ITCH-induced RASSF1A degradation at the PM (R9).

Besides SMAD and TEAD, YAP can also bind the transcriptional factor RUNX. Under normal conditions, RUNX can form complexes with YAP to promote ITCH's transcriptional expression and p73 degradation in several cell lines.[42,43] However, our experimental data in MCF-10A indicates the levels of both ITCH and p73 remained unaffected by TGF-β treatment over time (Figures S1F and S2A), implying the YAP-RUNX complex does not regulate ITCH and p73 in this context. This led us to exclude YAP-RUNX binding from our model. Similarly, while LATS1/2 phosphorylate YAP at S127 and retain it in the cytoplasm, our data shows that YAP-pS127 levels remained constant (Figure S1D) after TGF-β stimulation. Thus, the phosphorylation of YAP by LATS1/2 was also omitted from our model. These experimentally driven assumptions allowed us to simplify the model while preserving the most essential interactions critical for governing network dynamics.

Model implementation, calibration, and validation

Our new model was implemented using ordinary differential equations (ODEs). In this setup, the changes in the levels of model species are derived from reaction rates that are, in turn, defined using appropriate kinetic laws. A complete list of model ODEs and reaction rates are given in Tables S1–S3. To endow the model with context specificity and predictive power, we calibrated, i.e., trained, it using time-course experimental data obtained from MCF-10A cells (Figures 1B and 1D). This involved estimating unknown model parameters so that the model simulations recapitulate the data. We performed parameter estimation using genetic algorithm-based optimization in MATLAB, repeating this process 500 times to identify as many best-fitted parameter sets as possible (see STAR Methods and SI Text for details). Using multiple optimal parameter sets for model simulations prevents potential biases associated with a single optimal set, thereby enhancing model prediction reliability. Figure 2B shows that model simulations using the obtained best-fitted parameter sets accurately reflect the experimental data, as indicated by the high concordance between the simulated and actual data curves.

Model simulation correctly predicts the signaling effect of ITCH knockdown

To further substantiate the credibility of our model, we performed additional validation using independent experimental data. First, the model simulation predicts that an in silico knockdown of ITCH upregulates RASSF1A level in the absence of TGF-β stimulation (Figure 2C). To confirm this, we knocked down ITCH using siRNA and measured RASSF1A expression in MCF-10A cells using western blot (see STAR Methods). We obtained robust silencing of ITCH, and in agreement with the model prediction, ITCH silencing led to a clear increase in the RASSF1A level (Figure 2D). Furthermore, ITCH knockdown also resulted in the upregulation of PUMA, a marker of YAP-p73 transcriptional activity (Figure 2D). These results indicate that ITCH knockdown upregulates RASSF1A and augments YAP-p73 formation and transcriptional activity.

Next, we simulated the dynamics of RASSF1A in response to TGF-β stimulation under the ITCH knockdown condition. This showed no significant change in RASSF1A concentration at 8 and 24 h post TGF-β stimulation (Figure 2E). Model simulations indicate that in the context of ITCH knockdown (modeled as a 90% reduction in ITCH concentration), the interplay between RASSF1A degradation and its translocation to the plasma membrane upon TGF-β stimulation culminates in a relative stability in RASSF1A concentration. In the knockdown condition, the residual ITCH still contributes to a degree of RASSF1A degradation, leading to a decrease in total RASSF1A concentration. Conversely, TGF-β stimulation triggers the translocation of RASSF1A to the plasma membrane, effectively augmenting the total RASSF1A pool (considering both cytosolic and plasma membrane RASSF1A). These two opposing dynamics counter each other, resulting in minimal change in RASSF1A concentration at 8 and 24 h post TGF-β stimulation under ITCH knockdown. We tested this experimentally by knocking down ITCH and stimulating MCF-10A cells with TGF-β (Figure 2E). Consistent with the model prediction, no significant changes were observed in the level of RASSF1A under the ITCH knockdown condition. Collectively, these independent validations support the reliability and predictive capability of our model.

RASSF1A and ITCH coordinate switch-like transition of Yes-associated protein transcriptional complexes

RASSF1A is known to enhance the affinity between YAP and p73.[44] However, the coordination of YAP's complex formation with distinct transcriptional factors, such as p73 and SMAD, remains unclear. To address this, we investigated in silico the temporal and steady-state dynamics of the YAP-p73 and YAP-SMAD complexes under various network perturbations.

First, we performed model simulations where we systematically varied the synthesis rate of RASSF1A over an extensive range, and simulated the impact of this on the YAP-p73 and YAP-SMAD complexes at various time-points post TGF-β stimulation. The 3D model simulation revealed intricate dynamic properties of the system (Figures 3A and 3B). At both early and late time points, increasing RASSF1A levels
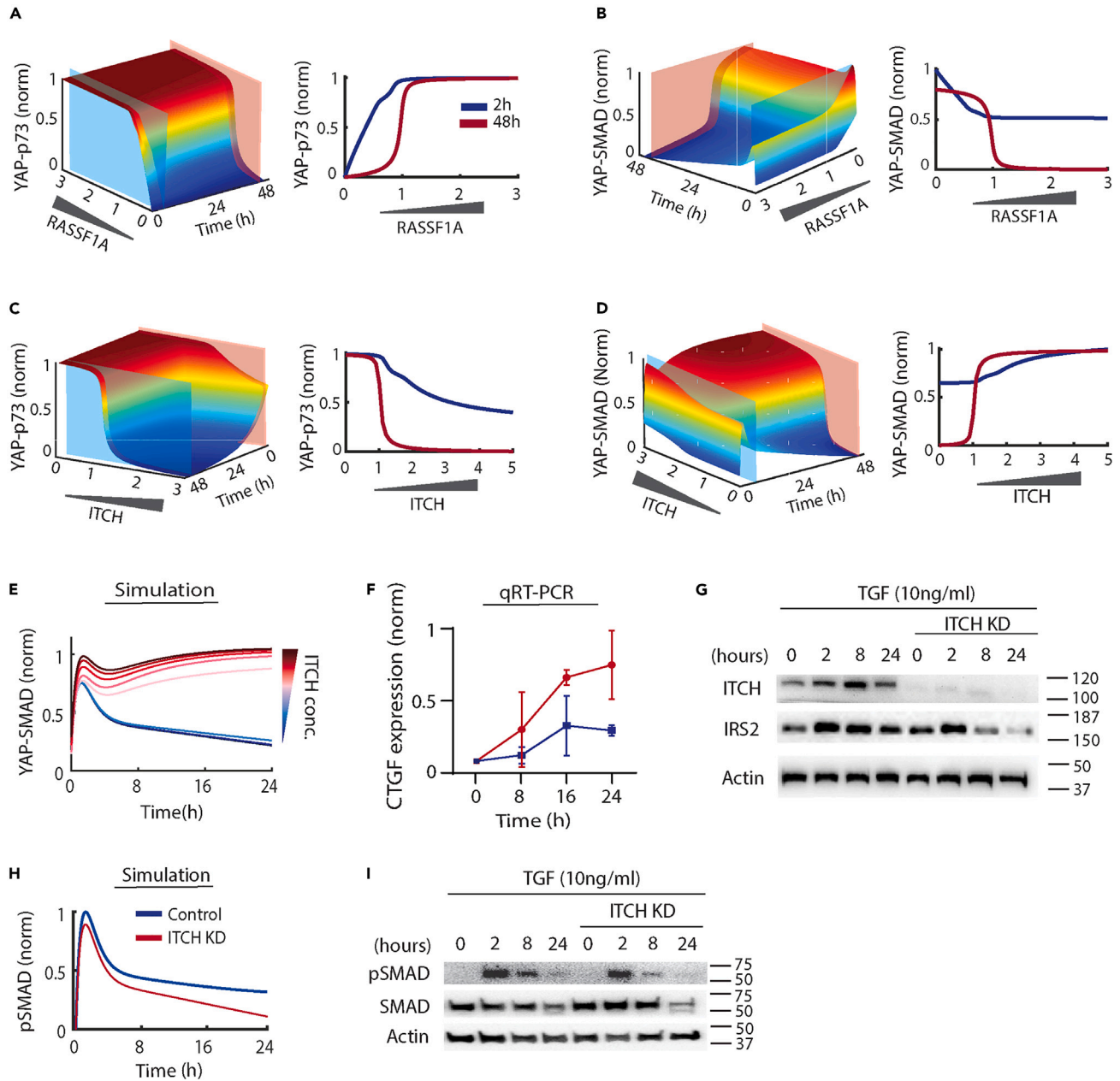
Figure 3. Molecular switches coordinate YAP-SMAD and YAP-p73 transcriptional complexes

(A–D) 3-dimendional (3D) model simulations of YAP-SMAD and YAP-p73 complex levels in response to TGF-β stimulation over time and simultaneous increase in RASSF1A (A-B) or ITCH levels (C-D). To simulate the variations in RASSF1A and ITCH levels, we increased the synthesis rate of RASSF1A and the total concentration of ITCH in the model from zero to three times their nominal values. This allowed us to explore a broad spectrum of concentrations for each protein. For each panel, the right side showcases a 2D simulation snapshot of dose-response curves influenced by RASSF1A (A, B) or ITCH (C, D). These snapshots compare early (2h, blue line) and late (48h, red line) time points following TGF-β stimulation.

(E) Upon TGF-β stimulation, model simulations reveal YAP-SMAD dynamics transitioning to sustained dynamics with increased ITCH levels, moving from low to high.

(F) Time-course expression of CTGF, a key transcriptional target gene of YAP-SMAD activity, under control (high ITCH) and ITCH-knockdown (low ITCH) conditions following TGF-β stimulation (10 ng/ml) in MCF-10A cells, measured using quantitative RT-PCR (n = 3 biological replicates). Error bars show mean ± standard deviation (SD).

(G) Time-course of IRS2 protein levels, another direct target of YAP-SMAD transcription, under control and ITCH-low conditions post-TGF-β stimulation, detected by Western blot (n = 3 biological replicates).

(H) Model simulations predicting ITCH knockdown reduces pSMAD levels.

(I) Temporal changes of pSMAD2 and total SMAD2 protein levels under control and ITCH-low conditions post TGF-β stimulation, detected by western blotting.

enhanced YAP-p73 but suppressed YAP-SMAD complex formation, consistent with the notion that SMAD and p73 compete for YAP. Interestingly, while a gradual increase in RASSF1A led to a linear-saturating rise in the YAP-p73 complex at 2 h, this response transformed into an abrupt switch-like pattern late time points, e.g., 48 h (Figure 3A). This behavior was mirrored inversely for the YAP-SMAD complex (Figure 3B). These switches imply a RASSF1A-gated threshold control mechanism: a slight increase in RASSF1A produces minimal effects on the complexes, but once a specific threshold is surpassed, RASSF1A triggers a surge in YAP-p73 and a plunge in the YAP-SMAD complex. In support of model prediction, our previous studies demonstrated that the gradual overexpression of RASSF1A indeed promoted YAP-p73 and simultaneously suppressed YAP-SMAD formation at 2 h post TGF-β stimulation in U2OS cells[27] (Figure S3A).

We previously showed that following TGF-β stimulation, RASSF1A and the E3 ligase ITCH are recruited to the PM by TGF-βR, where ITCH induces RASSF1A degradation.[27] This led us to postulate that ITCH might also regulates the dynamics of the YAP-TFs complexes. To examine this, we simulated the time-response of YAP complexes over 48-h span post TGF-β treatment across various ITCH expression levels. Simulations show that elevating ITCH levels switch on YAP-SMAD complex formation and switch off YAP-p73, but this switch is only pronounced at the late stage of TGF-β treatment. As a byproduct of the switch-like behavior, our simulations reveal that increasing ITCH levels transitions YAP-SMAD from a transient to a sustained dynamics. Low ITCH levels induce a peak-and-decline pattern for YAP-SMAD post TGF-β stimulation, whereas high levels sustain the increased YAP-SMAD concentration (Figures 3E and S3B).

To experimentally validate our model's predictions, we assessed the expression of CTGF, a target gene and common marker of YAP-SMAD transcriptional activity, over time following TGF-β stimulation. This was done using quantitative RT-PCR in MCF-10A cells under normal conditions and when ITCH was silenced using siRNA (Figure 3F). The data demonstrate a sustained increase in CTGF expression dynamics over 24 h post TGF-β stimulation with high ITCH levels. In contrast, when ITCH was knocked down, CTGF displayed significantly reduced and transient dynamics in response to TGF-β, peaking at 8 h and declining by 24 h. Beyond CTGF, we also measured the protein expression IRS2, another target gene of YAP,[45] following TGF-β stimulation. The immunoblotting assay revealed a pronounced decrease in IRS2 expression dynamics upon ITCH knockdown, further exhibiting a distinct transient pattern (Figures 3G and S3F). These experimental findings point to a shift from sustained to transient YAP-SMAD activity dynamics with decreasing ITCH levels, consistent with our model's predictions.

Mechanistically, the transition in YAP-SMAD dynamics is governed by two principal YAP interactions: YAP-p73 and YAP-SMAD, in our model. The YAP-p73 complex formation depends on RASSF1A levels, which increase when ITCH is low, facilitating YAP-p73 interaction. This scenario leads to a temporary rise in YAP-SMAD binding following TGF-β stimulation, as free YAP levels drop (see Figure 3E, blue lines). In contrast, high ITCH levels decrease RASSF1A, disrupt YAP-p73 complex formation, and allow more YAP to bind SMAD. This enhances and prolongs YAP-SMAD complex formation upon TGF-β stimulation (Figure 3E, red lines).

Next, we examined the impact of ITCH on TGF-β signaling using phosphorylated SMAD as a readout. Model simulations predict that knocking down ITCH reduces phosphorylated SMAD2 in response to TGF-β stimulation (Figure 3H). To validate this prediction, we assessed phosphorylated SMAD2 levels in both control and ITCH knockdown conditions using western blotting. Consistent with the model's prediction, the data reveal a transient response of pSMAD2 to TGF-β stimulation, which is diminished with ITCH knockdown (Figure 3I).

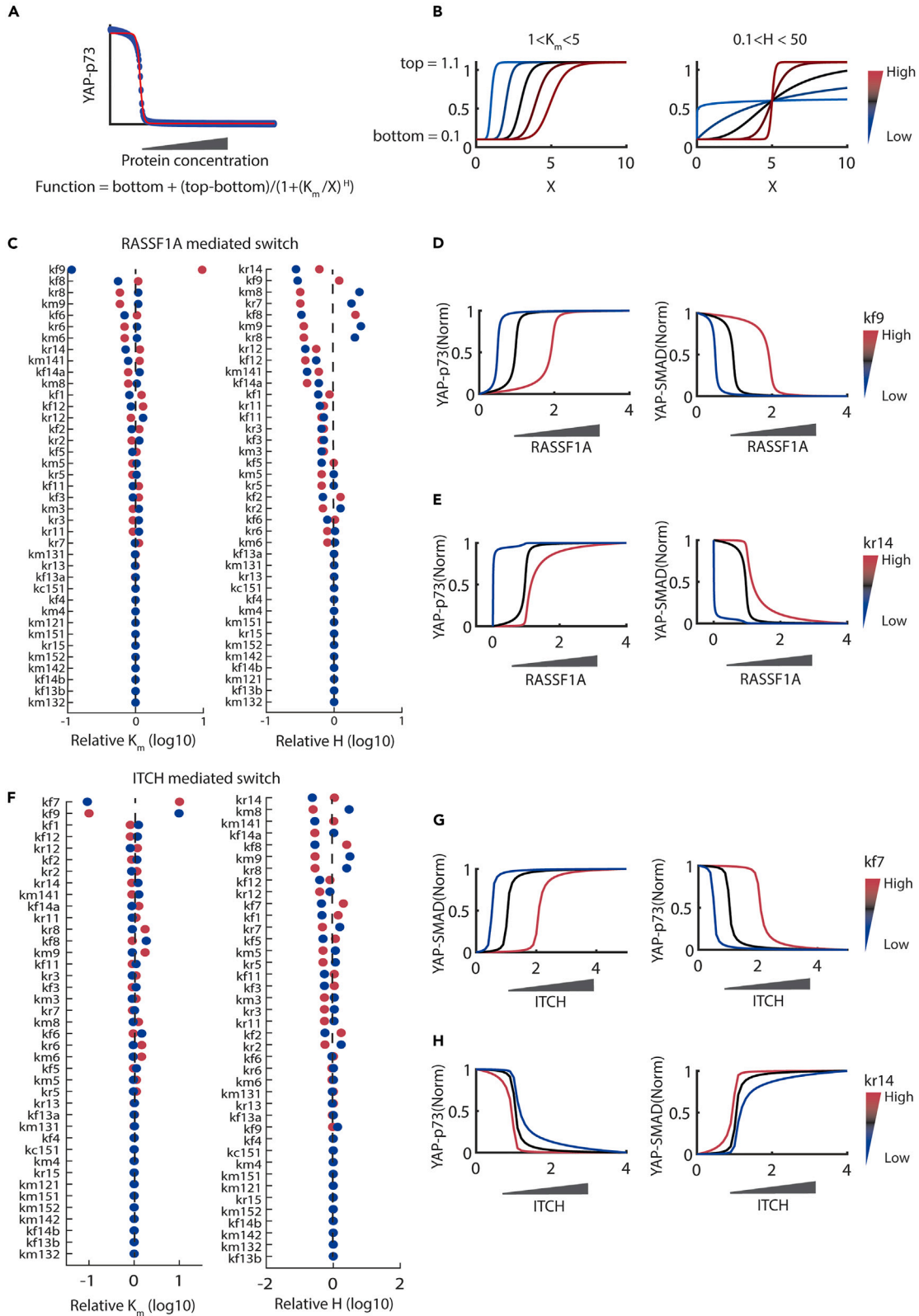### The emergence of Yes-associated protein transcriptional switches

Molecular switches often exhibit ultra-sensitivity due to positive feedback mechanisms[46,47] However, the observed YAP switches appear to emerge in the absence of explicit positive feedback loops. To dissect the wiring features that underpin the emergence of the YAP switches, we analyzed the underlying network structure. We postulated that the competition between SMAD and p73 for YAP binding might be the key factor behind these switch-like behaviors.

To investigate this, we developed two simplified 'toy' models to describe YAP's interaction with SMAD and p73 (Figures S3C and S3D). In Model I, YAP is represented in a single form capable of binding either SMAD or p73 (Figure S3C). Conversely, in Model II, YAP is characterised by two forms – unphosphorylated and phosphorylated. The unphosphorylated form primarily binds SMAD, while the phosphorylated form favors p73 (Figure S3D). This distinction in Model II closely reflects the situation in our comprehensive model (Figure 2A). We then subjected these models to extensive simulations with numerous randomly sampled parameter sets (varying both kinetic rates and state variables) to explore the potential behavior range of each model. We found that Model 1 consistently failed to generate steep switches in YAP complex levels in response to increasing kinetic parameters (e.g., YAP-p73 association rate, represented by kt1, Figure S3C, right). In contrast, Model II frequently exhibited switch-like behaviors across multiple parameter sets (Figure S3D, right). Quantifying the frequency and degree of the switches using a Hill coefficient confirms that unlike Model I, Model II is robust in generating steep switches (Figure S3E), aligning with our previous predictions using the detailed model. Collectively, our analysis suggests that the YAP transcriptional switches likely originate from the competitive, phosphorylation-mediated binding of YAP to its transcriptional partners, even in the absence of positive feedback regulation.

Network factors governing the behavior of Yes-associated protein transcriptional switches

Given the involvement of YAP in cancer, identifying the key factors that govern the YAP switches' behavior is important for understanding YAP-mediated cellular processes and their implications in cancer. Although such systematic analysis is experimentally challenging, our computationally model offers a feasible approach. We carried out a model-based 'sensitivity analysis', perturbing each kinetic parameter in the model by 10-fold either upward or downward relative to its nominal values. These kinetic parameters generally represent the strength of the network interactions they describe. We then assessed the subsequent impact on the switches' behavior.

A — YAP-p73 vs Protein concentration

Function = bottom + (top-bottom)/(1+(K_m/X)^H)

$$\text{Function} = \text{bottom} + (\text{top}-\text{bottom})/(1+(K_m/X)^H)$$

B — $1 < K_m < 5$ and $0.1 < H < 50$

C — RASSF1A mediated switch

D, **E** — YAP-p73(Norm), YAP-SMAD(Norm) vs RASSF1A; kf9, kr14

F — ITCH mediated switch

G, **H** — YAP-SMAD(Norm), YAP-p73(Norm) vs ITCH; kf7, kr14

Figure 4. Identification of network factors governing the YAP switches

(A) A schematic diagram depicting how the simulated YAP-TF response curves were fitted with a Hill function, in order to quantify the switches' salient properties, i.e., the switch steepness (parameter H) and threshold (parameter K_m).

(B) Simulations that illustrate indeed: increasing K_m results in a higher switching threshold, evidenced by the curve shifting to the right; while increasing H results in a steeper, more abrupt switch.

(C) Sensitivity analysis results for the RASSF1A-mediated switch. Each displayed kinetic parameter was systematically perturbed (i.e., 10-fold up or down from the nominal values), and the effects on the switch steepness and threshold were computed. Red dots indicate the effects resulting from increasing the parameters, whereas blue dots indicate the effects from decreasing the parameters.

(D) Simulation of the YAP-TF complexes in response to a gradual increase in RASSF1A level, at increasing values of the parameter k_{f9}.

(E) Simulation of the YAP-TF complexes in response to a gradual increase in RASSF1A level, at increasing values of the parameter k_{r14}.

(F) Sensitivity analysis results for the ITCH-mediated switch. Notations are the same as in (C).

(G) Simulation of the YAP-TF complexes in response to a gradual increase in ITCH level, at increasing values of the parameter k_{f7}.

(H) Simulation of the YAP-TF complexes in response to a gradual increase in ITCH level, at increasing values of the parameter k_{r14}.

To quantitatively measure the effect on the YAP switches, we fitted the simulated curve to a specialised function outlined in Figure 4A. Here, the parameter K_m represents the input threshold (in this case, ITCH or RASS1A) at which the curve toggles on or off, and H signifies the steepness of the switch. A higher H and K_m indicate a steeper switch and a greater switching threshold, respectively (Figure 4B).

Figure 4C displays the outcomes of the sensitivity analysis. Here, the kinetic parameters are ranked based on their influence on the RASSF1A-mediated switches. Interestingly, approximately a third of the tested parameters had negligible impact on either the switch's threshold or its steepness (Figure 4C). The degradation rate of RASSF1A (k_{f9}) has the most pronounced effect on the switching threshold, with an increasing in k_{f9} significantly elevating the RASSF1A level needed to activate YAP-p73 and deactivate YAP-SMAD (Figure 4D). Next to k_{f9}, the rates that govern RASSF1A's translocation to and from the PM (k_{f8}/k_{r8}) emerge as the next significant determinants for the threshold (Figure 4C). Notably, we observed that the dissociation rate of YAP-p73 (k_{r14}) most strongly influences the steepness for both RASSF1A- and ITCH-mediated YAP switches (Figures 4C and 4F). Suppressing this rate transitions the YAP-p73/SMAD responses from a switch-like to a more gradual pattern (Figures 4E and 4H).
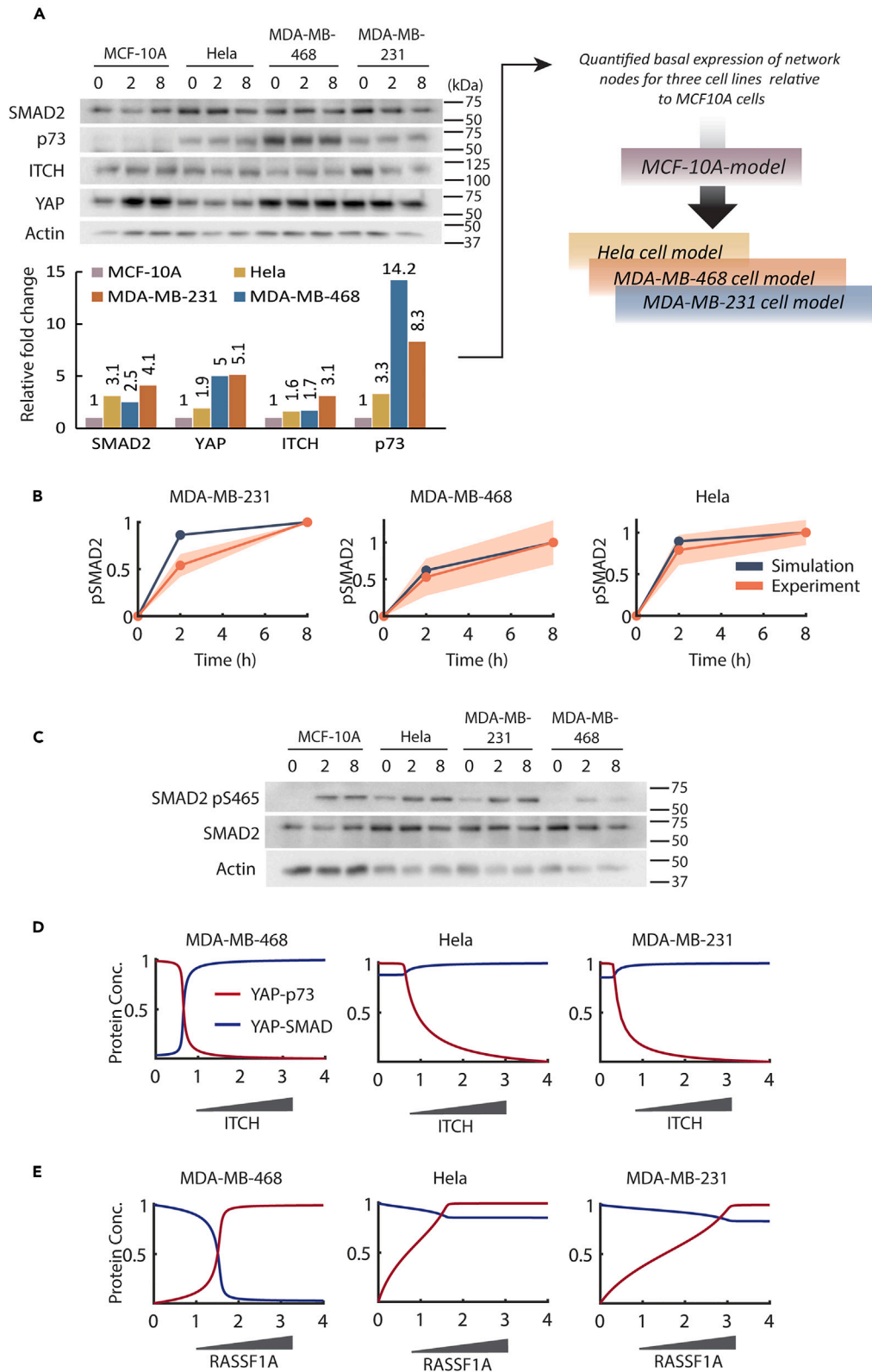
Furthermore, our findings highlight that RASSF1A's synthesis rate (k_{f7}) most dramatically impacts the threshold for the ITCH-mediated YAP switches. Raising RASSF1A's synthesis rate potently shifts the YAP-SMAD on-switch and YAP-p73 off-switch to the right (Figure 4G), meaning higher ITCH levels are required to trigger the switches. This is because as k_{f7} increases, greater ITCH levels are needed to degrade the more abundant RASSF1A below the critical threshold for the switches to take place (Figure S4A, dashed line). Consistent with this data, boosting RASSF1A's degradation rate (k_{f9}) induces the reverse effect (Figure 4F). Together, these observations suggest that when RASSF1A is overexpressed, cells necessitate a higher ITCH concentration to activate YAP-SMAD and the subsequent proliferative transcription mechanism. In contrast, in tumor with RASSF1A downregulation, it is likely cells would not need as much ITCH to trigger YAP-SMAD. In fact, when analysing the co-expression patterns of RASSF1 and ITCH across extensive breast and pan-cancer patients datasets, it is evident that patients with downregulated RASSF1 rarely show ITCH overexpression compared to those with normal or upregulated RASSF1 (Figure S4B), consistent with our predictions.

Interrogation of the Yes-associated protein switches across diverse cell types

Given that variations in protein expression influences signaling response,[48] we sought to determine how heterogeneity in protein profiles across different cell types may impact the behavior of the YAP switches. We first measured the basal protein expression of key network components in three additional breast cancer cell lines: HeLa, MDA-MB-231 and MDA-MB-468 (Figure 5A). Data quantification, normalized to MCF-10A cells, revealed considerable variability in protein expression across the different cell lines (Figure 5A). Notably, MDA-MB-468 expresses a significantly high abundance of p73, approximately 15, 5 and 2-folds higher than in MCF-10A, HeLa and MDA-MB-231, respectively. Both MDA-MB-231 and MDA-MB-468 exhibit YAP expression level that are around 2–3 times higher than those in MCF-10A and HeLa cells. Conversely, HeLa and MDA-MB-231 have the highest basal levels of SMAD2. However, all four cell lines display similar levels of ITCH expression (Figure 5A). These data highlight the pronounced variability in the abundance of network components, which could lead to distinct network dynamic behaviors across the cell types.

Using the relative expression fold-changes from above, we adapted the MCF-10A model for three other cell lines, adjusting the concentration of relevant model species accordingly. For instance, given YAP is 5-fold more abundant in MDA-MB-231 than MCF-10A, its level in the corresponding model was increased 5-fold. This customization approach has been effective in previous studies.[2,49,50] Consequently, we derived three distinct models tailored for HeLa, MDA-MB-231, and MDA-MB-468. To verify these models with independent data not utilized during the customization, we simulated the dynamic response of phosphorylated SMAD2 to TGF-β stimulation for each model and conducted corresponding time-course experiments to corroborate model predictions (Figures 5B and 5C). The simulations aligned well with the increasing and sustained trends seen in the data (Figure 5B), confirming the models' predictive accuracy.

Using these cell-specific models for simulation, we examined the YAP-TFs switches in the new cell lines. Interestingly, while RASSF1A and ITCH regulate the transition between YAP complexes consistently across cell types, the simulations show distinct quantitative behaviors in terms of switch steepness and threshold. For instance, the ITCH-mediated YAP switches are most pronouncedly sigmoidal in MDA-MB-468, with the lowest switching threshold in MDA-MB-231 (Figure 5D). Moreover, the YAP complex responses to RASSF1A are more gradual in HeLa and MDA-MB-231 cells compared to MDA-MB-468 (Figure 5E). Overall, these results suggest the presence of the on/off-switches of

A

Quantified basal expression of network nodes for three cell lines relative to MCF10A cells

MCF-10A-model

Hela cell model

MDA-MB-468 cell model

MDA-MB-231 cell model

B

C

D

E

Figure 5. Cell type-specific models predict context dependent signaling activation and switch behaviors

(A) Comparative analysis of the basal expression of various network components and their response to 8 h of TGF-β (10 ng/ml) across MCF-10A and different breast cancer cell types (HeLa, MDA-MB-468 and MDA-MB-231) using western blot (upper panel) (n = 1 biological replicates). Quantification of the data (above) showing the total basal expression of the network components in MDA-MB-468, MDA-MB-231 and HeLa cells relative to that in MCF-10A cells (lower panel). A schematic showing how the relative protein expression data were used to customize the MCF-10A model to generate models for the MDA-MB-468, MDA-MB-231 and HeLa cell lines (right pannel).

(B) Time-course model prediction of phosphorylated SMAD2 in response to TGF-β stimulation in specific cell types using the models constructed in (A), and validates against corresponding experimental data quantified from (C). The orrange line indicates mean and the shaded area indicates the standard deviation of three experimental replicates (see also Figure S5).

(C) Comparative time-course analysis of TGF-β stimulation (10 ng/mL) on phosphorylated and total levels of SMAD2 in four different cell lines (n = 3 biological replicates).

(D and E) Model simulations of the formation and transition between the YAP-TF complexes using the cell type-specific models, which demonstrate highly context-dependent switching behavior. To perturb ITCH and RASSF1A levels *in silico*, the total concentration of ITCH and synthesis rate of RASSF1A were perturbed from zero to 4-fold higher than their nominal values.

YAP-TFs complexes coordinated by ITCH and RASSF1A across diverse cell types. However, the specific behavior of these switches is dictated by the protein expression profiles unique to each cell type. Importantly, our models serve as a valuable tool for predicting the context-specific behavior of these switches.

ITCH's influence on Yes-associated protein activities is closely tied to its role in cell viability

Our earlier analysis shows ITCH regulates YAP transcriptional complexes differently across cellular contexts. For example, ITCH strongly modulates YAP-SMAD/p73 formation in MDA-MB-468 and MCF-10A cells, but more subtly in MDA-MB-231 and HeLa cells (Figure 5D). Given that unique YAP-TFs complexes steer varied transcriptional outcomes, we hypothesized a connection ITCH's control over these complexes and its overall functional significance.

To test this, we gauged ITCH's importance in cell viability using the 'essentiality score' from the DEPMAP data portal.[29] The portal catalogs essentiality scores (ranging from −1 to 1) based on gene deletion impact on cell viability across 342 cell lines: −1 indicates high essentiality, 0 denotes neutrality, and 1 suggests gene loss boosts cell viability. To discern if ITCH's essentiality correlates with its influence on YAP activities, we obtained protein expression data for 375 human cancer cell lines from the CCLE consortium.[51] Among these, 54 displayed detectable key model components (Figure 6A) and were selected for further analysis. Using the model customization previously outlined, we constructed 54 cell lines-specific models and simulated the ITCH-mediated YAP switches for each (Figure 6B). Simulations revealed that the YAP switch-like responses consistently manifest across numerous cell lines, but their amplitude and threshold vary. We formulated an 'ITCH impact score' to quantify the ITCH's effect on YAP complexes and thus activity regulation (shown in Figure 6A). A higher score means a stronger ITCH influence on YAP regulation.

For the 36 cell lines featured in both DEPMAP and CCLE, a correlation analysis between the essentiality and impact scores revealed a significant negative correlation (correlation-coefficient = −0.44, p value = 0.006), suggesting that YAP's pivotal role in mediating cell viability directly aligns with its potent regulation of transcriptional complexes. This underscores a tangible link between ITCH's mediation of YAP activities and its biological significance.

DISCUSSION

Experimental evidence suggests YAP can both regulate proliferative and apoptotic programs in cells, but the mechanisms by which YAP mediates its context-dependent function is unclear. The TGF-β signaling pathway, upon activation, engages YAP to drive oncogenic transcription through the YAP-SMAD complex. Conversely, the Hippo pathway, via RASSF1A, initiates apoptotic transcription by promoting YAP-p73 binding. Due to the intricate crosstalk between these pathways, YAP might preferentially assemble with specific transcriptional factors based on the network state, potentially influencing tumor progression. However, the coordination of opposing YAP transcriptional complexes at the network level has not been characterized, mainly due to the lack of integrative frameworks to navigate this complexity. In this study, we present new mathematical models describing complex TGF-β/Hippo pathway interplay and undertook integrative modelling-experimental analysis to study YAP-TFs complex dynamics across cellular contexts.

Past mathematical models of the TGF-β and Hippo pathways were built separately by various teams, including ours.[2,19,32,33] For example, an ODE model by Zi et al. examined time- and dose-dependent TGF-β effects [33], revealing a switch-like pSMAD2 response during prolonged TGF-β exposure, contrasting with its short-term linear counterpart. This distinction may influence cell-fate decisions. Nicklas et al. explored the TGF-β pathway dynamics, focusing on the SMAD1/2 phosphorylation and its association with SMAD4.[32] Our models of the Hippo pathway previously shed light on its interactions with pathways including RAF-1/ERK and AKT, identifying molecular switches.[2,19] However, these models only accounted for the signaling events upstream of YAP and did not include YAP. A more recent model considered TGF-β and YAP crosstalk,[40] however, it overlooked the intricate dynamics involving YAP complexes and RASSF1A/ITCH-mediated crosstalk. Thus, the new model in this study emerges as the pioneering experimentally validated representation that intricately maps the mechanistic interplay between the TGF-β and Hippo-YAP pathways, particularly emphasizing the distinct YAP-TF complexes.

Our integrative studies have, for the first time, identified molecular switches that regulate the competing formation of YAP-SMAD and YAP-p73 complexes. As these complexes direct opposing gene expression programs, the identified switches likely offer a mechanism for cells
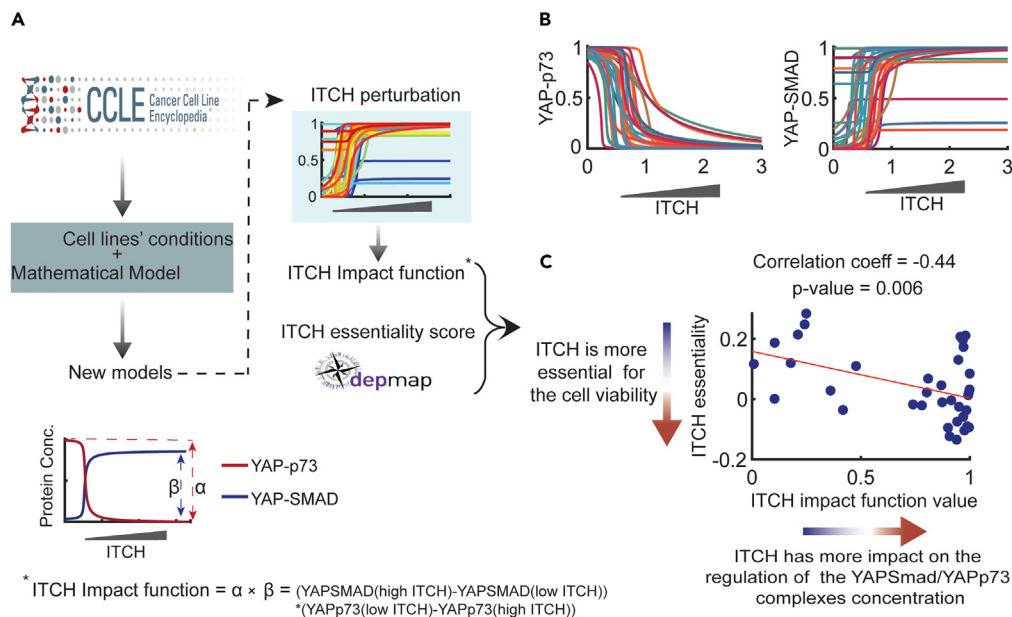
Figure 6. The impact of ITCH in the regulation of YAP activities is linked to its essentiality in cell viability

(A) A workflow used to simulate the ITCH-mediated YAP switches in multiple cancer cell lines using data from the CCLE database, and compute ITCH's impact on YAP regulation. Briefly, CCLE database was used to find the initial condition of the components of model for 375 different cell lines. Among them 54 cell lines express detectable levels of the model components and thus were selected for further analysis. Using these initial conditions the existing model is adjusted to the 54 cell lines. *ITCH impact score* is defined and calculated for each cell line. ITCH essentiality score for the cell viability is also obtained for 342 cell lines using DEPMAP bio-portal. There are 36 cell lines that overlap between the DEPMAP and CCLE databases (i.e., having both essentiality and impact scores for ITCH). A more detailed description is given in STAR Methods.

(B) Simulation of the ITCH-dependent switches of YAP complexes in different cell lines using cell type specific models generated in (A). To perturb ITCH levels *in silico*, the total concentration of ITCH in each specific cell line model was changed from zero to 3-folds higher than the nominal values. Model simulations predict the presence of abrupt switch-like response of the YAP-TF complexes.

(C) A significant and strong correlation is recorded between the ITCH impact function values and ITCH's essentiality score across 36 different cell lines.

to decisively opt for distinct cellular outcomes, such as cell proliferation or death, under the influence of YAP. It is well established that living cells frequently employ molecular switches to dictate cell fate decisions.[52–54] Examples include bistable switches arising from positive feedback,[55,56] and sigmoidal switches stemming from non-feedback regulation.[2,57] We found that RASSF1A and ITCH play vital roles in controlling these YAP-TF switches. Specifically, an incremental rise in RASSF1A expression can trigger a sudden increase in the formation of the apoptotic YAP-p73 complex, simultaneously causing a sharp decrease in the proliferative YAP-SMAD complex. In contrast, ITCH functions in an opposite manner. This aligns with the known tumor-suppressing role of RASSF1A in various cancers.[58] In addition, the competition between SMAD and p73 for YAP binding highlights the threshold-driven transition of YAP between the complexes. When ITCH expression surpasses a certain threshold, YAP shifts from predominantly binding with p73 to associating with SMAD. This transition amplifies proliferative gene expression while suppressing apoptotic gene expression. This coordinated toggle, facilitated by YAP between opposing complexes, likely reinforces the precision of cellular decision-making processes.

Consequent to the switch-like behavior observed in our simulations, we predicted that increasing ITCH levels would transition YAP-SMAD activity from a transient to a sustained dynamic, a prediction we subsequently validated experimentally. This shift in YAP-SMAD dynamics hold several implications. Previous research has shown that alterations in signaling dynamics can direct cellular outcomes.[59,60] For example, in PC12 cells, epidermal growth factor (EGF) induces a transient ERK activation, resulting in cell proliferation. In contrast, nerve growth factor (NGF) triggers sustained ERK activation, leading to cell differentiation.[61] Thus, the shift in YAP-SMAD dynamics suggests that ITCH might modulate cellular reactions to TGF-β stimulation, potentially impacting cellular fates such as proliferation or apoptosis. Furthermore, given the established links between disruptions in the YAP-SMAD pathway and diseases such as cancer, elucidating the role of ITCH in this pathway can offer insights into disease progression and potential therapeutic avenues. For example, therapeutics could be designed to modulate ITCH levels, thereby controlling YAP-SMAD dynamics.

Our model-based approach offers the advantage of systematically analyzing emergent behaviors *in silico* that are experimentally challenging to address. Through model simulations, we pinpointed the core network motif responsible for the observed switches. Sensitivity analysis further identified key kinetic parameters that govern the quantitative features of the YAP switches. We determined that the competitive, phosphorylation-mediated binding of YAP to its transcriptional partners drives the switches without requiring explicit positive feedback. Moreover, the degradation rate of RASSF1A primarily determines the switching threshold, while the dissociation rate of the YAP-p73 complex most affects the switch steepness. These findings underscore computational models' value in elucidating intricate regulators within complex

signaling networks. Additionally, to validate the robustness of out models against variations in the type of reaction rates used, we constructed an alternative model employing Michaelis-Menten kinetics for phosphorylation and dephosphorylation reactions (Table S4). Following recalibration with the same experimental dataset (Figure S7 and Table S5), the switch-like behavior predicted by this model aligned with our primarily model's predictions. This consistency highlights the independence of our simulations from the specific reaction rate formalisms employed, reinforcing the robustness of our findings.

In exploring the context-specificity of the YAP switches, we extended our analysis beyond MCF-10A cells to other breast cancer cell lines. Our simulations, guided by the characterization of protein expression in these cells, revealed that while the core behavior of YAP switches was conserved, the details of the switching threshold and steepness were uniquely determined by the specific cellular context. For example, ITCH perturbation elicited more abrupt switches in MDA-MB-468 cells but smoother transitions in HeLa and MDA-MB-231 cells. This underlines the significant role of the cellular environment in shaping the dynamics of YAP transcriptional complexes and emphasize the need for the careful consideration of network contexts in studying these intricate regulatory mechanisms. Such findings deepen our understanding of cell-to-cell variability and may have implications for targeted therapeutic intervention where YAP signaling plays a vital role.

Our findings underscore the oncogenic potential of ITCH by modulating YAP activities (Figures 3C and 3D). The variable YAP responses across cell lines to ITCH perturbation (Figure 5D) prompted us to examine any correlation with ITCH's impact on cell viability. Using DEPMAP portal's gene essentiality score combined with cell line-specific CCLE protein expression profiles, we identified a strong correlation between ITCH's influence on YAP regulation and its essentiality across cell lines (Figure 6C). This connection amplifies the role of ITCH-mediated YAP switches in cellular functions. Our findings complement existing literature, reporting ITCH as an oncogenic factor in multiple malignancies.[61–65] Its overexpression in breast cancer, for example, promotes metastasis and is linked to poor survival rate.[31] In addition, data from The Cancer Genome Atlas indicates elevated levels of ITCH in several other cancers, including rectal adenocarcinoma, and uterine carcinoma (Figure S6). Consequently, targeting ITCH emerges as a potential therapeutic avenue for the treatment of specific cancers.[30]

Limitations of the study

While our study offers significant insights into the coordination of YAP transcriptional complexes and activities, several limitations must be acknowledged. The reliance on mathematical models, while valuable, can introduce biases or oversimplifications that might not always fully capture the intricacies of cellular dynamics under specific contexts. In addition, while our simulation studies have revealed intriguing insights into the crosstalk network's systems behaviors, some findings await experimental confirmation. Future research could, for instance, rigorously validate the presence of YAP switches in various cellular contexts and *in vivo*. Nevertheless, the insights provided here set a valuable groundwork for subsequent research.

STAR★METHODS

Detailed methods are provided in the online version of this paper and include the following:

- KEY RESOURCES TABLE
- RESOURCE AVAILABILITY
  - ○ Lead contact
  - ○ Materials availability
  - ○ Data and code availability
- EXPERIMENTAL MODEL AND STUDY PARTICIPANT DETAILS
  - ○ Cell culture
  - ○ siRNA and transfection
  - ○ Immunoblotting
  - ○ Quantitative RT-PCR analysis
- METHOD DETAILS
  - ○ Mathematical modelling
  - ○ Model calibration (parameter estimation)
  - ○ Customizing the Hippo-TGF-β model for different cell line conditions
- QUANTIFICATION AND STATISTICAL ANALYSIS

SUPPLEMENTAL INFORMATION

Supplemental information can be found online at https://doi.org/10.1016/j.isci.2024.109031.

REFERENCES

1. Meng, Z., Moroishi, T., and Guan, K.-L. (2016). Mechanisms of Hippo pathway regulation. Genes Dev. 30, 1–17.

2. Romano, D., Nguyen, L.K., Matallanas, D., Halasz, M., Doherty, C., Kholodenko, B.N., and Kolch, W. (2014). Protein interaction switches coordinate Raf-1 and MST2/Hippo signalling. Nat. Cell Biol. 16, 673–684.

3. Zhang, N., Bai, H., David, K.K., Dong, J., Zheng, Y., Cai, J., Giovannini, M., Liu, P., Anders, R.A., and Pan, D. (2010). The Merlin/NF2 tumor suppressor functions through the YAP oncoprotein to regulate tissue homeostasis in mammals. Dev. Cell 19, 27–38.

4. Dupont, S., Morsut, L., Aragona, M., Enzo, E., Giulitti, S., Cordenonsi, M., Zanconato, F., Le Digabel, J., Forcato, M., Bicciato, S., et al. (2011). Role of YAP/TAZ in mechanotransduction. Nature 474, 179–183.

5. Stein, C., Bardet, A.F., Roma, G., Bergling, S., Clay, I., Ruchti, A., Agarinis, C., Schmelzle, T., Bouwmeester, T., Schübeler, D., and Bauer, A. (2015). YAP1 exerts its transcriptional control via TEAD-mediated activation of enhancers. PLoS Genet. 11, e1005465.

6. Calses, P.C., Crawford, J.J., Lill, J.R., and Dey, A. (2019). Hippo pathway in cancer: aberrant regulation and therapeutic opportunities. Trends Cancer 5, 297–307.

7. Zhao, B., Wei, X., Li, W., Udan, R.S., Yang, Q., Kim, J., Xie, J., Ikenoue, T., Yu, J., Li, L., et al. (2007). Inactivation of YAP oncoprotein by the Hippo pathway is involved in cell contact inhibition and tissue growth control. Genes Dev. 21, 2747–2761.

8. Zhang, X., Abdelrahman, A., Vollmar, B., and Zechner, D. (2018). The ambivalent function of YAP in apoptosis and cancer. Int. J. Mol. Sci. 19, 3770.

9. Zhao, B., Ye, X., Yu, J., Li, L., Li, W., Li, S., Yu, J., Lin, J.D., Wang, C.-Y., Chinnaiyan, A.M., et al. (2008). TEAD mediates YAP-dependent gene induction and growth control. Genes Dev. 22, 1962–1971.

10. Fujii, M., Toyoda, T., Nakanishi, H., Yatabe, Y., Sato, A., Matsudaira, Y., Ito, H., Murakami, H., Kondo, Y., Kondo, E., et al. (2012). TGF-β synergizes with defects in the Hippo pathway to stimulate human malignant mesothelioma growth. J. Exp. Med. 209, 479–494.

11. Hiemer, S.E., Szymaniak, A.D., and Varelas, X. (2014). The transcriptional regulators TAZ and YAP direct transforming growth factor β-induced tumorigenic phenotypes in breast cancer cells. J. Biol. Chem. 289, 13461–13474.

12. Qiao, Y., Lin, S.J., Chen, Y., Voon, D.C.C., Zhu, F., Chuang, L.S.H., Wang, T., Tan, P., Lee, S.C., Yeoh, K.G., et al. (2016). RUNX3 is a novel negative regulator of oncogenic TEAD–YAP complex in gastric cancer. Oncogene 35, 2664–2674.

13. Kulkarni, M., Tan, T.Z., Syed Sulaiman, N.B., Lamar, J.M., Bansal, P., Cui, J., Qiao, Y., and Ito, Y. (2018). RUNX1 and RUNX3 protect against YAP-mediated EMT, stem-ness and shorter survival outcomes in breast cancer. Oncotarget 9, 14175–14192.

14. Strano, S., Munarriz, E., Rossi, M., Castagnoli, L., Shaul, Y., Sacchi, A., Oren, M., Sudol, M., Cesareni, G., and Blandino, G. (2001). Physical interaction with Yes-associated protein enhances p73 transcriptional activity. J. Biol. Chem. 276, 15164–15173.

15. Matallanas, D., Romano, D., Yee, K., Meissl, K., Kucerova, L., Piazzolla, D., Baccarini, M., Vass, J.K., Kolch, W., and O'Neill, E. (2007). RASSF1A elicits apoptosis through an MST2 pathway directing proapoptotic transcription by the p73 tumor suppressor protein. Mol. Cell 27, 962–975.

16. Romano, D., Matallanas, D., Weitsman, G., Preisinger, C., Ng, T., and Kolch, W. (2010). Proapoptotic kinase MST2 coordinates signaling crosstalk between RASSF1A, Raf-1, and Akt. Cancer Res. 70, 1195–1203.

17. Guo, C., Zhang, X., and Pfeifer, G.P. (2011). The tumor suppressor RASSF1A prevents dephosphorylation of the mammalian STE20-like kinases MST1 and MST2. J. Biol. Chem. 286, 6253–6261.

18. O'Neill, E., Rushworth, L., Baccarini, M., and Kolch, W. (2004). Role of the kinase MST2 in suppression of apoptosis by the proto-oncogene product Raf-1. Science 306, 2267–2270.

19. Shin, S.-Y., and Nguyen, L.K. (2016). Unveiling hidden dynamics of hippo signalling: A systems analysis. Genes 7, 44.

20. Kim, M., and Jho, E.-H. (2014). Cross-talk between Wnt/β-catenin and Hippo signaling pathways: a brief review. BMB Rep. 47, 540–545.

21. Vališ, K., and Novák, P. (2020). Targeting ERK-Hippo interplay in cancer therapy. Int. J. Mol. Sci. 21, 3236.

22. Grannas, K., Arngården, L., Lönn, P., Mazurkiewicz, M., Blokzijl, A., Zieba, A., and Söderberg, O. (2015). Crosstalk between Hippo and TGFβ: subcellular localization of YAP/TAZ/Smad complexes. J. Mol. Biol. 427, 3407–3415.

23. Futakuchi, A., Inoue, T., Wei, F.-Y., Inoue-Mochita, M., Fujimoto, T., Tomizawa, K., and Tanihara, H. (2018). YAP/TAZ are essential for TGF-β2–mediated conjunctival fibrosis. Invest. Ophthalmol. Vis. Sci. 59, 3069–3078.

24. Qin, Z., Xia, W., Fisher, G.J., Voorhees, J.J., and Quan, T. (2018). YAP/TAZ regulates TGF-β/Smad3 signaling by induction of Smad7 via AP-1 in human skin dermal fibroblasts. Cell Commun. Signal. 16, 1–12.

25. Varelas, X., Sakuma, R., Samavarchi-Tehrani, P., Peerani, R., Rao, B.M., Dembowy, J., Yaffe, M.B., Zandstra, P.W., and Wrana, J.L. (2008). TAZ controls Smad nucleocytoplasmic shuttling and regulates human embryonic stem-cell self-renewal. Nat. Cell Biol. 10, 837–848.

26. Varelas, X., Samavarchi-Tehrani, P., Narimatsu, M., Weiss, A., Cockburn, K., Larsen, B.G., Rossant, J., and Wrana, J.L. (2010). The Crumbs complex couples cell density sensing to Hippo-dependent control of the TGF-β-SMAD pathway. Dev. Cell 19, 831–844.

27. Pefani, D.-E., Pankova, D., Abraham, A.G., Grawenda, A.M., Vlahov, N., Scrace, S., and O'Neill, E. (2016). TGF-β targets the hippo pathway scaffold RASSF1A to facilitate YAP/SMAD2 nuclear translocation. Mol. Cell 63, 156–166.

28. Feng, X.-H., and Derynck, R. (2005). Specificity and versatility in TGF-β signaling through Smads. Annu. Rev. Cell Dev. Biol. 21, 659–693.

29. Meyers, R.M., Bryan, J.G., McFarland, J.M., Weir, B.A., Sizemore, A.E., Xu, H., Dharia, N.V., Montgomery, P.G., Cowley, G.S., Pantel, S., et al. (2017). Computational

correction of copy number effect improves specificity of CRISPR–Cas9 essentiality screens in cancer cells. Nat. Genet. *49*, 1779–1784.

30. Li, P.-F., and Zhang, Q.-G. (2018). Inhibition of ITCH Suppresses Proliferation and Induces Apoptosis of Lung Cancer Cells. Cell. Physiol. Biochem. *48*, 1703–1709.

31. Salah, Z., Itzhaki, E., and Aqeilan, R.I. (2014). The ubiquitin E3 ligase ITCH enhances breast tumor progression by inhibiting the Hippo tumor suppressor pathway. Oncotarget *5*, 10886–10900.

32. Nicklas, D., and Saiz, L. (2013). Computational modelling of Smad-mediated negative feedback and crosstalk in the TGF-β superfamily network. J. R. Soc. Interface *10*, 20130363.

33. Zi, Z., Feng, Z., Chapnick, D.A., Dahl, M., Deng, D., Klipp, E., Moustakas, A., and Liu, X. (2011). Quantitative analysis of transient and sustained transforming growth factor-β signaling dynamics. Mol. Syst. Biol. *7*, 492.

34. Levy, D., Adamovich, Y., Reuven, N., and Shaul, Y. (2008). Yap1 phosphorylation by c-Abl is a critical step in selective activation of proapoptotic genes in response to DNA damage. Mol. Cell *29*, 350–361.

35. Keshet, R., Adler, J., Ricardo Lax, I., Shanzer, M., Porat, Z., Reuven, N., and Shaul, Y. (2015). c-Abl antagonizes the YAP oncogenic function. Cell Death Differ. *22*, 935–945.

36. Li, B., He, J., Lv, H., Liu, Y., Lv, X., Zhang, C., Zhu, Y., and Ai, D. (2019). c-Abl regulates YAP Y357 phosphorylation to activate endothelial atherogenic responses to disturbed flow. J. Clin. Invest. *129*, 1167–1179.

37. Wilkes, M.C., and Leof, E.B. (2006). Transforming growth factor β activation of c-Abl is independent of receptor internalization and regulated by phosphatidylinositol 3-kinase and PAK2 in mesenchymal cultures. J. Biol. Chem. *281*, 27846–27854.

38. Khatibi, S., Zhu, H.-J., Wagner, J., Tan, C.W., Manton, J.H., and Burgess, A.W. (2017). Mathematical model of tgf-βsignalling: feedback coupling is consistent with signal switching. BMC Syst. Biol. *11*, 48.

39. Vizán, P., Miller, D.S.J., Gori, I., Das, D., Schmierer, B., and Hill, C.S. (2013). Controlling long-term signaling: receptor dynamics determine attenuation and refractory behavior of the TGF-β pathway. Sci. Signal. *6*, ra106.

40. Labibi, B., Bashkurov, M., Wrana, J.L., and Attisano, L. (2020). Modeling the Control of TGF-β/Smad Nuclear Accumulation by the Hippo Pathway Effectors, Taz/Yap. iScience *23*, 101416.

41. Yan, X., Liu, Z., and Chen, Y. (2009). Regulation of TGF-β signaling by Smad7. Acta Biochim. Biophys. Sin. *41*, 263–272.

42. Rossi, M., Aqeilan, R.I., Neale, M., Candi, E., Salomoni, P., Knight, R.A., Croce, C.M., and Melino, G. (2006). The E3 ubiquitin ligase Itch controls the protein stability of p63. Proc. Natl. Acad. Sci. USA *103*, 12753–12758.

43. Levy, D., Reuven, N., and Shaul, Y. (2008). A regulatory circuit controlling Itch-mediated p73 degradation by Runx. J. Biol. Chem. *283*, 27462–27468.

44. García-Gutiérrez, L., McKenna, S., Kolch, W., and Matallanas, D. (2020). RASSF1A Tumour Suppressor: Target the Network for Effective Cancer Therapy. Cancers *12*, 229.

45. Wang, C., Jeong, K., Jiang, H., Guo, W., Gu, C., Lu, Y., and Liang, J. (2016). YAP/TAZ regulates the insulin signaling via IRS1/2 in endometrial cancer. Am. J. Cancer Res. *6*, 996–1010.

46. Ferrell, J.E., and Ha, S.H. (2014). Ultrasensitivity part II: multisite phosphorylation, stoichiometric inhibitors, and positive feedback. Trends Biochem. Sci. *39*, 556–569.

47. Nguyen, L.K., and Kholodenko, B.N. (2016). Feedback Regulation in Cell Signalling: Lessons for Cancer Therapeutics (Elsevier), pp. 85–94.

48. Norris, D., Yang, P., Shin, S.-Y., Kearney, A.L., Kim, H.J., Geddes, T., Senior, A.M., Fazakerley, D.J., Nguyen, L.K., James, D.E., and Burchfield, J.G. (2021). Signaling Heterogeneity is Defined by Pathway Architecture and Intercellular Variability in Protein Expression. iScience *24*, 102118.

49. Shin, S.-Y., Müller, A.K., Verma, N., Lev, S., and Nguyen, L.K. (2018). Systems modelling of the EGFR-PYK2-c-Met interaction network predicts and prioritizes synergistic drug combinations for triple-negative breast cancer. PLoS Comput. Biol. *14*, e1006192.

50. Ghomlaghi, M., Yang, G., Shin, S.Y., James, D.E., and Nguyen, L.K. (2021). Dynamic modelling of the PI3K/MTOR signalling network uncovers biphasic dependence of mTORC1 activity on the mTORC2 subunit SIN1. PLoS Comput. Biol. *17*, e1008513.

51. Nusinow, D.P., Szpyt, J., Ghandi, M., Rose, C.M., McDonald, E.R., 3rd, Kalocsay, M., Jané-Valbuena, J., Gelfand, E., Schweppe, D.K., Jedrychowski, M., et al. (2020). Quantitative Proteomics of the Cancer Cell Line Encyclopedia. Cell *180*, 387–402.e16. https://doi.org/10.1016/j.cell.2019.12.023.

52. Ferrell, J.E., and Machleder, E.M. (1998). The biochemical basis of an all-or-none cell fate switch in Xenopus oocytes. Science *280*, 895–898.

53. Ferrell, J.E., Jr., Pomerening, J.R., Kim, S.Y., Trunnell, N.B., Xiong, W., Huang, C.-Y.F., and Machleder, E.M. (2009). Simple, realistic models of complex biological processes: positive feedback and bistability in a cell fate switch and a cell cycle oscillator. FEBS Lett. *583*, 3999–4005.

54. Tyson, J.J., Chen, K.C., and Novak, B. (2003). Sniffers, buzzers, toggles and blinkers: dynamics of regulatory and signaling pathways in the cell. Curr. Opin. Cell Biol. *15*, 221–231.

55. Byrne, K.M., Monsefi, N., Dawson, J.C., Degasperi, A., Bukowski-Wills, J.-C., Volinsky, N., Dobrzyński, M., Birtwistle, M.R., Tsyganov, M.A., Kiyatkin, A., et al. (2016). Bistability in the Rac1, PAK, and RhoA signaling network drives actin cytoskeleton dynamics and cell motility switches. Cell Syst. *2*, 38–48.

56. Nguyen, L.K., Muñoz-García, J., Maccario, H., Ciechanover, A., Kolch, W., and Kholodenko, B.N. (2011). Switches, excitable responses and oscillations in the Ring1B/Bmi1 ubiquitination system. PLoS Comput. Biol. *7*, e1002317.

57. Varusai, T.M., Kolch, W., Kholodenko, B.N., and Nguyen, L.K. (2015). Protein–protein interactions generate hidden feedback and feed-forward loops to trigger bistable switches, oscillations and biphasic dose–responses. Mol. Biosyst. *11*, 2750–2762.

58. Malpeli, G., Innamorati, G., Decimo, I., Bencivenga, M., Nwabo Kamdje, A.H., Perris, R., and Bassi, C. (2019). Methylation dynamics of RASSF1A and its impact on cancer. Cancers *11*, 959.

59. Kiyatkin, A., van Alderwerelt van Rosenburgh, I.K., Klein, D.E., and Lemmon, M.A. (2020). Kinetics of receptor tyrosine kinase activation define ERK signaling dynamics. Sci. Signal. *13*, eaaz5267.

60. Ryu, H., Chung, M., Dobrzyński, M., Fey, D., Blum, Y., Lee, S.S., Peter, M., Kholodenko, B.N., Jeon, N.L., and Pertz, O. (2015). Frequency modulation of ERK activation dynamics rewires cell fate. Mol. Syst. Biol. *11*, 838.

61. Yin, Q., Wyatt, C.J., Han, T., Smalley, K.S., and Wan, L. (2020). ITCH as a Potential Therapeutic Target in Human Cancers (Elsevier).

62. Ishihara, T., Tsuda, H., Hotta, A., Kozaki, K.i., Yoshida, A., Noh, J.Y., Ito, K., Imoto, I., and Inazawa, J. (2008). ITCH is a putative target for a novel 20q11. 22 amplification detected in anaplastic thyroid carcinoma cells by array-based comparative genomic hybridization. Cancer Sci. *99*, 1940–1949.

63. Salah, Z., Melino, G., and Aqeilan, R.I. (2011). Negative regulation of the Hippo pathway by E3 ubiquitin ligase ITCH is sufficient to promote tumorigenicity. Cancer Res. *71*, 2010–2020.

64. Ho, K.C., Zhou, Z., She, Y.-M., Chun, A., Cyr, T.D., and Yang, X. (2011). Itch E3 ubiquitin ligase regulates large tumor suppressor 1 stability. Proc. Natl. Acad. Sci. USA *108*, 4870–4875.

65. Rossi, M., De Laurenzi, V., Munarriz, E., Green, D.R., Liu, Y.C., Vousden, K.H., Cesareni, G., and Melino, G. (2005). The ubiquitin–protein ligase Itch regulates p73 stability. EMBO J. *24*, 836–848.

66. Kim, J.H., Zhang, T., Wong, N.C., Davidson, N., Maksimovic, J., Oshlack, A., Earnshaw, W.C., Kalitsis, P., and Hudson, D.F. (2013). Condensin I associates with structural and gene regulatory regions in vertebrate chromosomes. Nat. Commun. *4*, 2537.

67. Geiger, T., Wehner, A., Schaab, C., Cox, J., and Mann, M. (2012). Comparative proteomic analysis of eleven common cell lines reveals ubiquitous but varying expression of most proteins. Mol. Cell. Proteomics *11*. M111.014050.

68. Lawrence, R.T., Perez, E.M., Hernández, D., Miller, C.P., Haas, K.M., Irie, H.Y., Lee, S.-I., Blau, C.A., and Villén, J. (2015). The proteomic landscape of triple-negative breast cancer. Cell Rep. *11*, 630–644.

STAR★METHODS

KEY RESOURCES TABLE

REAGENT or RESOURCE	SOURCE	IDENTIFIER
Software and algorithms		
MATLAB	MathWorks	https://www.mathworks.com/
Adobe illustrator	Adobe	https://www.adobe.com/products/illustrator.html
Fiji ImageJ	Schindelin et al., 2012	https://scicrunch.org/resolver/RRID:SCR_003070
IQM	IntiQuan	https://iqmtools.intiquan.com/
Graphpad Prism	GraphPad Software Inc.	https://www.graphpad.com/
Rotor-Gene Q	Qiagen	https://www.qiagen.com/kr/resources/resourcedetail?id=8435805b-2c5d-4fa9-948c-a43de75a7ee1&lang=en
ImageLab	Bio-Rad	https://www.bio-rad.com/en-au/product/image-lab-software?ID=KRE6P5E8Z
Github	GitHub, Inc.	https://github.com/NguyenLab-IntegratedNetworkModeling/TGF_Hippo_crosstalk.
Antibodies		
pSMAD2 (S465/467)	Cell Signalling Technology	CST #3108; RRID:AB_490941
SMAD2	Cell Signalling Technology	CST #3122; RRID:AB_823638
YAP	Cell Signalling Technology	CST #14074; RRID:AB_2650491
pYAP (Y357)	Abcam	ab62751; RRID:AB_956486
pYAP (S127)	Cell Signalling Technology	CST #13008; RRID:AB_2650553
pSMAD3 (S423/S425)	Cell Signalling Technology	CST #9520; RRID:AB_2193207
SMAD7 (ab216428)	Abcam	ab216428; RRID:AB_2889839
RASSF1A	ThermoFisher Scientific	#14-6888-82; RRID:AB_468373
β-actin	Sigma-Aldrich	A1978; RRID:AB_476692
14-3-3	Santa Cruz Biotechnology	SC-1657; RRID:AB_626618
Experimental models: Cell lines		
HeLa	American Type Culture Collection	RRID: CVCL_0030
MCF-10A	American Type Culture Collection	RRID: CVCL_0598
MDA-MB-231	American Type Culture Collection	RRID: CVCL_0062
MDA-MB-468	American Type Culture Collection	RRID: CVCL_0419
Chemicals, peptides, and recombinant proteins		
Bovine Insulin	Sigma-Aldrich	I0516-5ML
Insulin	Novo Nordisk	Actrapid HM
Cholera toxin	Sigma-Aldrich	C8052-1MG
Hydrocortisone	Sigma-Aldrich	H0888-5G
EGF	R&D systems	#236-EG

(Continued on next page)

Continued

REAGENT or RESOURCE	SOURCE	IDENTIFIER
HEPES	Invitrogen	#15630080
Horse serum	Invitrogen	#16050122
Fetal Bovine Serum	Scientifix PTY LTD	FBSFR-S00JF
TGF-β	STEMCELL technologies	#100-0856
ON-TARGET plus SMARTpool ITCH siRNA	Millennium Science PTY LTD	#13014
OTP Non-Targeting Control	Millennium Science PTY LTD	#13017
Critical commercial assays		
TransIT-X2	Mirus Bio	MIR6004
Pierce™ BCA Protein Assay Kit	ThermoFisher	#23225
Monarch Total RNA Miniprep Kit	New England Biolabs	T2010S
High Capacity cDNA Reverse Transcription Kits	ThermoFisher	#4368814
QuantiNova SYBR Green PCR Kit	Qiagen	#208052
Deposited data		
Proteomics IBAQ database	Geiger et al.	https://doi.org/10.1074/mcp.M111.014050
Triple-negative breast cancer proteomics database	Lawrence et al.	https://doi.org/10.1016/j.celrep.2015.04.059

RESOURCE AVAILABILITY

Lead contact

Further information and requests for resources and reagents should be directed to and will be fulfilled by the lead contact, Dr Lan K Nguyen (lan.k.nguyen@monash.edu).

Materials availability

This study did not generate new unique reagents.

Data and code availability

- All data reported in this paper will be shared by the lead contact upon request.
- The relevant code has been archived on GitHub and can be accessed at: https://github.com/NguyenLab-IntegratedNetworkModeling/TGF_Hippo_crosstalk.
- Any additional information required to reanalyze the data reported in this paper is available from the lead contact upon request.

EXPERIMENTAL MODEL AND STUDY PARTICIPANT DETAILS

Cell culture

MCF-10A cells obtained from the ATCC (USA) were cultured in Dulbecco's Modified Eagle Medium /nutrient mixture F-12 (Invitrogen) with 5% (v/v) horse serum (Invitrogen), 0.5% μg/ml hydrocortisone (Sigma), 10 μg/ml bovine insulin (Sigma), 100 ng/ml cholera toxin (Sigma) and 20 ng/ml human recombinant EGF (R&D Systems). HeLa, MDA-MB-231 and MDA-MB-468 cells were obtained from ATCC (USA) and maintained in RPMI 1640 media (Gibco) with 10% (v/v) Fetal Bovin Serum, 10 μg/ml Insulin and 20 mM HEPES. All cells grew in incubators with a humidified atmosphere containing 5% CO_2 and 95% air at 37°C.

siRNA and transfection

MCF10A cells were transfected with 20 nM ON-TARGETplus SMARTpool ITCH siRNA (#13014, Millennium Science PTY LTD) with 20 nM OTP Non-Targeting Control (#13017, Millennium Science PTY LTD) as controls, using *Trans*IT-X2 (Mirus Bio) according to manufacturer's instructions.

Immunoblotting

Immunoblotting was conducted as describe in.[66] In brief, cells were lysed with RIPA lysis buffer supplemented with 10 μg/mL Aprotinin, 10 μg/mL Leupeptin, 1 mM PMSF and 1 mM sodium orthovanadate. Protein concentration was quantified using Pierce™ BCA Protein Assay

Kit following the manufacturer's protocol.[65] Forty micrograms protein from each sample ws resolved on 10% SDS-PAGE gels. Primary antibodies were pSMAD2 (S465/467) (CST #3108), SMAD2 (CST #3122), YAP (CST #14074), pYAP (Y357) (ab62751), pYAP (S127) (CST #13008), pSMAD3 (S423/S425) (CST #9520), SMAD7 (ab216428) and RASSF1A (eB114-10H1) (ebioscience #14-6888-82). β-actin (Sigma A1978) or 14-3-3 (sc-1657) were used as loading controls. Secondary antibodies were anti-rabbit IgG-HRP or anti-mouse IgG-HRP. Immobilon® Crescendo Western HRP Substrate (Merck) was used according to the manufacturer's instruction.

Quantitative RT-PCR analysis

ITCH were knockdown by transfecting 20 nM ON-TARGET plus SMARTpool ITCH siRNA with 20 nM OTP as controls in MCF-10A cells. 48 hours later, these cells were subjected for a second transfection overnight but in media without serum. Serum starved ITCH knockdown and OTP control cells were stimulated with 10ng/mL TGF-β, cells were harvested at 0h, 2h, 8h and 24h.The quantitative RT-PCR analysis was conducted as described.[67] Briefly, total RNAs were extracted from TGF-β stimulated ITCH knockdown cells and OTP control cells using Monarch Total RNA Miniprep Kit (T2010S, NEB) according to the manufacturer's instruction. Total RNA (2 μg) from each sample was reverse transcribed with High Capacity cDNA Reverse Transcription Kits (ThermoFisher) according to the manufacturer's protocols. All cDNA samples were diluted to 5 ng/μl for qRT-PCR analysis. cDNA (5 ng) of each sample was amplified using QuantiNova SYBR Green PCR Kit (Qiagen) according to manufacturer's protocol. Primers used are as follow. CTGF-For: 5' CCA ATG ACA ACG CCT CCT G 3', CTGF-Rev: 5' TGG TGC AGC CAG AAA GCT C 3', CYR61-For: 5' GAG TGG GTC TGT GAC GAG GAT 3', CYR61-Rev: 5' GGT TGT ATA GGA TGC GAG GCT 3', GAPDH-For: 5' GGA GCG AGA TCC CTC CAA AAT 3', GAPDH-Rev: 5' GGC TGT TGT CAT ACT TCT CAT GG 3'. The amplification was conducted using Rotor-Gene Q real-time PCR cycler (Qiagen). The relative quantification of the interested gene expression was calculated using $2^{-\Delta\Delta Ct}$ method after the threshold cycle (Ct) was normalised with the Ct of GAPDH. At least three different experiments were performed individually, and each sample was run in triplicates.

METHOD DETAILS

Mathematical modelling

We developed a mathematical model to represent the crosstalk between Hippo and TGF-β pathways. Biochemical reactions were formulated using ordinary differential equations (ODEs), often referred to as chemical kinetic equations. Detailed reaction rates and ODEs can be found in Tables S1 and S2, and the best-fitted parameter sets utilised for simulations are provided in Data S1. Model construction, calibration, and simulations were implemented in MATLAB (The MathWorks. Inc. 2020b).

To accurately simulate the network's dynamic response to perturbations, such as TGF-β stimulation, we first ran the model under unperturbed conditions for a sufficient duration to reach a steady state. Following this, we introduced specific perturbations to study the system's reactions. This 'priming' ensured that the initial conditions of the simulation reflected the cell state before perturbation, aligning with the experimental setup.

Model calibration (parameter estimation)

To estimate model parameters during model calibration, we employed an objective function J that quantifies the discrepancy between the model's simulation outcomes and the quantified experimental data:

$$J(p) = \sum_{j=1}^{M} \sum_{i=1}^{N} \left(y_{j,i}^{D} - y_j(t_i, p) \right)^2$$

In this equation, M denotes the number of experimental data sets used for fitting, and N signifies the number of time points within each set. The term $y_j(t_i, p)$ indicates the simulation of component j at the time point t_i with parameter set p applied. The term $y_{j,i}^{D}$ is the experimental data for component j at the time point t_i. The parameters were fine-tuned to minimize the objective function J. This was done using the Global Optimization Toolbox with the genetic algorithm 'ga' function in MATLAB, setting a population size of 200 and a generation number of 800. The initial conditions in our model were derived from the intensity-based absolute quantification (iBAQ) experimental data for MCF10A cell lines, as detailed in this study by Lawrence et al..[68] iBAQ is a method used in mass spectrometry-based proteomics to estimate the absolute quantity of individual proteins within a sample. In our study, these iBAQ values offered a robust and reliable measure of the protein concentrations in the MCF10A cells under non-stimulated conditions. We thus used these values as the initial conditions for our model, preceding the application of TGF-beta stimulation. Moreover, for model calibration and parameter estimation, the time-course experimental data shown in Figures 1B and 1D were quantified and utilised.

Acknowledging the possibility of multiple optimal parameter sets fitting the experimental data, we repeated the genetic algorithm procedure 500 times independently. This was to identify the broadest range of best-fitted sets for subsequent ensemble simulations. We established a selection criterion where the objective function values of these sets had to be below a cut-off threshold. Consequently, we opted for 11 best-fitted parameter sets for further simulation and analysis. The relevant code and parameter sets have been archived on GitHub and can be accessed at: https://github.com/NguyenLab-IntegratedNetworkModeling/TGF_Hippo_crosstalk.

Customizing the Hippo-TGF-β model for different cell line conditions

To adapt the Hippo-TGF-β model to different cell lines, we modified initial conditions based on protein expressions:

Using western blot data: For specificity to cell lines, such as HeLa, MDA-MB-468, and MDA-MB-231, we incorporated protein expression ratios relative to MCF-10A cells derived from in-house Western blot data (Figure 5A). The formula for the level of protein x in cell line y is:

$$= Relative\ protein\ concentration\ from\ western\ blot\ data \left(\frac{cell\ line\ y}{MCF10A}\right) \times protein\ concentration\ in\ MCF10A\ cell\ line$$

Using CCLE protein expression data: To further adapt our model for the diverse biological conditions of cancer cell lines, we used cell-type-specific protein expression data. First, we collected relative protein expression data for 375 human cancer cell lines from CCLE. Then, to determine absolute protein levels, we referred to a dataset by Geiger et al.,[67] which included *absolute* protein abundances for 11 cell lines, derived from mass spectrometry and the iBAQ (intensity-based absolute quantification) algorithm. Seven cell lines appeared in both datasets, allowing us to use their iBAQ data combined with the *relative* CCLE expressions to estimate absolute protein levels for the CCLE cell lines. For instance, we calculated absolute protein abundances for 341 cell lines by correlating their CCLE data with the iBAQ data of MCF7. We replicated this method for the other six cell lines with iBAQ data. Consequently, we generated seven inferred protein abundance sets for each of the 342 CCLE cell lines, averaging them to define final protein concentrations. These averages updated our model's initial conditions to tailor it for each of the 342 cancer cell lines. The following formula is used to infer the absolute protein abundance of the proteins of interest (network proteins) for each of the 342 cancer cell lines in the CCLE database:

$$Protein\ concentration\ (i,x) = \frac{1}{7} \sum_{j=1}^{7} IBAQ\ (i,j) \times \frac{CCLE\ (i,x)}{CCLE\ (i,j)}$$

$$= \frac{\frac{IBAQ\ (i,MCF7)}{CCLE\ (i,MCF7)} + \frac{IBAQ\ (i,U2OS)}{CCLE\ (i,U2OS)} + ... + \frac{IBAQ\ (i,A549)}{CCLE\ (i,A549)}}{7} \times CCLE\ (i,x)$$

Here *i* and *x* denote protein *i* in cell line *x* (one of the 342 CCLE cell lines). The absolute abundance of protein *i* in cell line *j* is represented by *IBAQ(i, j)*, where *j* represents one of the seven cell lines from the iBAQ dataset: *j* = (*MCF7, U2OS, LnCap, RKO, K562, HepG2 or A549*); and *CCLE(i, j)* is the relative expression of protein *i* in cell line *j* from the CCLE database. For more details please see [50]. Note that since 54 of the 342 CCLE cell lines have detectable levels of the key network nodes, only these 54 cell lines were used for model customization. Finally, the MDA-MB-468 cell line, part of the CCLE cohort and previously modelled using our Western blot data, served as a benchmark. We adjusted this benchmark model's initial conditions to create specific models for the remaining 53 suitable cell lines.

QUANTIFICATION AND STATISTICAL ANALYSIS

All data were analysed using GraphPad Prism 9.0 (GraphPad, San Diego, CA, USA) and shown as mean ± standard deviation (SD). Continuous data differences analysis was evaluated by Student's t-test between two groups. One-way analysis of variance (ANOVA) test was used to analyse differences among multiple groups. $P<0.05$ was considered significant. ns $P>= 0.05$, *$P < 0.05$, **$P < 0.01$, ***$P < 0.001$, ****$P < 0.0001$. Statistical details for each experiment are included in the figures and figure legends.

Densitometry analysis of the immunoblots was performed on the detected bands using ImageLab, version 5.2.1 (Bio-Rad). The intensity of each band was normalised against the intensity of their corresponding loading control. Bands correlating to phospho-proteins were further normalised to the bands of corresponding total protein levels.